



# 1 On the regional-scale streamflow variability using flow 2 duration curve

3 Pankaj Dey<sup>1</sup>, Jeenu Mathai<sup>2</sup>, Murugesu Sivapalan<sup>3,4</sup> and Pradeep. P. Mujumdar<sup>5,6</sup>

4 <sup>1</sup>Department of Hydrology, Indian Institute of Technology, Roorkee, India

5 <sup>2</sup>National Centre for Earth Science Studies, Thiruvananthapuram, India

6 <sup>3</sup>Department of Civil and Environmental Engineering, University of Illinois at Urbana-Champaign, Urbana, IL,  
7 USA

8 <sup>4</sup>Department of Geography and Geographic Information Science, University of Illinois at Urbana-Champaign,  
9 Urbana, IL, USA

10 <sup>5</sup>Department of Civil Engineering, Indian Institute of Science, Bangalore, India

11 <sup>6</sup>Interdisciplinary Centre for Water Research, Indian Institute of Science, Bangalore, India

12

13 *Correspondence to:* Pankaj Dey ([pdev609@gmail.com](mailto:pdev609@gmail.com))

14

15 **Abstract.** As each catchment responds uniquely, even if they appear similar, formulating generalizable  
16 hypotheses and using routinely used signatures of catchment similarity to examine streamflow variability can be  
17 difficult. Flow Duration Curve (FDC), a concise portrayal of streamflow variability at a specific gauging station,  
18 can provide insights into hydroclimatic and landscape processes occurring at a wide range of space and time scales  
19 that govern flow regimes in a region. This study explores the suitability of partitioning of annual streamflow FDC  
20 into seasonal FDCs, and total streamflow FDC into fast and slow flow FDCs to unravel the process controls on  
21 FDCs at a regional scale, with application to low-gradient rivers flowing east from the Western Ghats of  
22 Peninsular India. The focus is on investigation of the controls of common regional landscape features (in space)  
23 and seasonal climatic (in time) variations on regional variations of the FDC. Findings of the study indicate that  
24 bimodal rainfall seasonality and higher fraction of moderate to good groundwater potential zones explains the  
25 higher contribution of slow flow to total flow across north-south gradient of the region. Shapes of fast and slow  
26 FDCs are controlled by recession parameters revealing the role of climate seasonality and geologic profiles,  
27 respectively. A systematic spatial variation across north-south gradient is observed– highlighting the importance  
28 of coherent functioning of landscape-hydroclimate settings in imparting distinct signature of streamflow  
29 variability. The framework is useful to discover the role of time and process controls on streamflow variability in  
30 a region with seasonal hydroclimatology and hydro-geologic gradients.

## 31 1 Introduction

32 The hydrologic functioning of catchment systems in any given region is coevolved with the long-term climatology  
33 and landscape features present in the region through mutual interactions operating across multiple spatial and  
34 temporal scales (Wagner et al., 2013). These interactions and long-term feedbacks impart variability to  
35 hydrologic processes that are characteristic of the region of interest, including runoff generation and riverine  
36 transport processes, thus influencing water availability and reliability to human populations that depend on the  
37 streamflow. Understanding streamflow variability in time and space across river basins in the region is therefore



38 very important for water resource management (Deshpande et al., 2016; Sinha et al., 2018) and the prediction and  
39 mitigation of floods (Kale et al., 1997). The frequency of high flows, low flows, or flows within specific ranges,  
40 is essential for risk assessment of water management projects involving control of streamflow variability. Correct  
41 portrayal of streamflow variability at the scale of catchments and river basins is therefore an indispensable  
42 component in many hydrologic applications.

43 The focus of this paper is on the flow duration curve (FDC), which is a compact description of temporal  
44 streamflow variability at the catchment scale. The FDC represents (daily) streamflow values plotted against the  
45 proportion of time the given flow is exceeded or equalled (Smakhtin, 2001; Vogel & Fennessey, 1994). The  
46 graphical form of the FDC embeds within it the governing hydrologic processes and dominant flow characteristics  
47 throughout the range of recorded streamflows at the catchment scale (Botter et al., 2008). In this sense, the FDC  
48 is also an important signature of a catchment's rainfall to runoff transformation (Ghotbi et al., 2020a; Vogel &  
49 Fennessey, 1994). FDC thus typifies the old proverb, "one picture is worth a thousand words" with its potential  
50 to encapsulate much of the relevant information of streamflow variability in a single plot (Vogel & Fennessey,  
51 1995), and has been used in many hydrologic applications. Vogel and Fennessey (1994) provide a brief history of  
52 the application of flow duration curves in hydrology. Applications of FDC include waste load allocation (Searcy,  
53 1959), water quality management (Searcy, 1959; Rehana & Mujumdar, 2011, 2012), reservoir and sedimentation  
54 studies (Vogel & Fennessey, 1995), low-flow and flood analyses (Smakhtin, 2001), assessment of environmental  
55 flow requirements (Smakhtin and Anputhas, 2006), and water availability for hydropower (Basso & Botter, 2012).

56 Streamflow observed in a river is the culmination of interacting hydrological processes of runoff generation,  
57 overland and subsurface flow and evaporation, operating at multiple time and space scales, in response to climatic  
58 inputs and their interactions with a range of landscape properties, all of which are highly heterogeneous. This  
59 makes it challenging to decipher the process controls on streamflow variability, and their manifestation in the  
60 shape of the FDC (Cheng et al., 2012; Ghotbi et al., 2020b; Yokoo & Sivapalan, 2011). Therefore, there is a need  
61 for appropriate conceptual frameworks that can bring out these process controls of FDCs and generate deep  
62 insights into the governing principles underpinning observed variability. Yokoo and Sivapalan (2011) presented  
63 a framework for deciphering the process controls of the FDC by considering the FDC of total streamflow (TFDC)  
64 as a statistical summation of a fast flow duration curve (FFDC) and a slow flow duration curve (SFDC). FFDC is  
65 a filtered version of precipitation variability, with rainfall intensity patterns and surface soil characteristics as  
66 controlling factors (Yokoo & Sivapalan, 2011). On the other hand, SFDC reflects a competition between  
67 subsurface drainage and evapotranspiration (Yokoo & Sivapalan, 2011), in which case seasonality and regional  
68 geology are stronger controlling factors. This contrast in the process controls governing quick (surface) runoff  
69 and slow (subsurface) flow, supports the notion of stratifying total streamflow into these two components  
70 operating at two different time scales. The distinction between the two (fast and slow) flow time scales enables  
71 the conceptualization of the process controls of fast flow (surface runoff) and slow flow (subsurface streamflow  
72 and groundwater flow) separately (Cheng et al., 2012; Yokoo & Sivapalan, 2011).

73 Ghotbi et al (2020a, 2020b) used this framework to explore the climatic and landscape controls of FDCs using  
74 streamflow data for hundreds of catchments across the continental United States in a comparative manner. In  
75 their work Ghotbi et al. (2020a) emphasized the need to consider the fast flow and slow flow time series  
76 independently as stochastic responses of catchments to sequences of storm events. Intensity and frequency of



77 rainfall events and the properties of soils and topography govern the variability of fast flows, whereas climate  
78 seasonality and regional geology of the aquifer system govern variability of slow flow components. More  
79 specifically, Ghotbi et al. (2020b) showed the dominant process controls of FDCs as aridity index, topographic  
80 slope, coefficient of variation of daily precipitation, timing of rainfall, time interval between storms, snow fraction,  
81 and recession slope.

82 Due to significant differences between fast and slow process controls, each may be used to explain streamflow  
83 variability independently. While recognizing the necessity to represent the hydrological processes across two  
84 distinct time scales, this paper aims to develop a process-based understanding of how regional scale features  
85 impact streamflow variability across Peninsular India, using the flow duration curve (FDC) as a signature of this  
86 variability. For this purpose, an extension of this concept was made by including seasonal (timing) streamflow  
87 variability in a regional context. To isolate the effects of the drivers on the observed FDCs and to identify the  
88 controls of time and process scales on streamflow variability, a modeling framework is presented that comprises  
89 partitioning streamflow in multiple ways: seasons/months in the time domain, east-west/north-south directions in  
90 the space domain, fast/slow flows in the process domain. Streamflow data available from a large number of stream  
91 gauges within and between the major river basins across Peninsular India is employed for this purpose. The  
92 scientific novelty and methodological advancement of the paper lie in two interconnected aspects, which have not  
93 been adopted in the literature to date: (i) the timescale partitioning framework is used to study the relative  
94 contributions of different seasons to the FDC (repeated for fast and slow flow components), exploring how the  
95 relative contributions holistically vary across the whole region and using the framework to reconstruct the annual  
96 flow duration curve using seasonal flow duration curves, (ii) the Wegenerian approach in connecting the spatial  
97 variability of streamflow at a regional scale using flow duration curve. Thus, the main goal of this paper is to  
98 reconstruct the flow duration curves at different scales to unravel the regional scale streamflow variability by  
99 extending the process partitioning (Ghotbi et al., 2020a) with the time partitioning. Studies that use simultaneous  
100 partitioning of flow duration curves at seasonal and process scales to investigate regional streamflow variability  
101 in space and seasonal climatic in time fluctuations using the Wegenerian approach are limited. The remainder of  
102 the paper is structured as follows. Section 2 elaborates on the details of the study area and the daily streamflow  
103 dataset used. The description of the conceptual framework employed for the analysis is presented in Section 3.  
104 The results of the application of the framework to Peninsular India and the interpretation of the results are  
105 presented in Sections 4 and 5, respectively. Finally, the paper is concluded in Section 6 with key insights gained  
106 for the nature and controls of streamflow variability across Peninsular India.

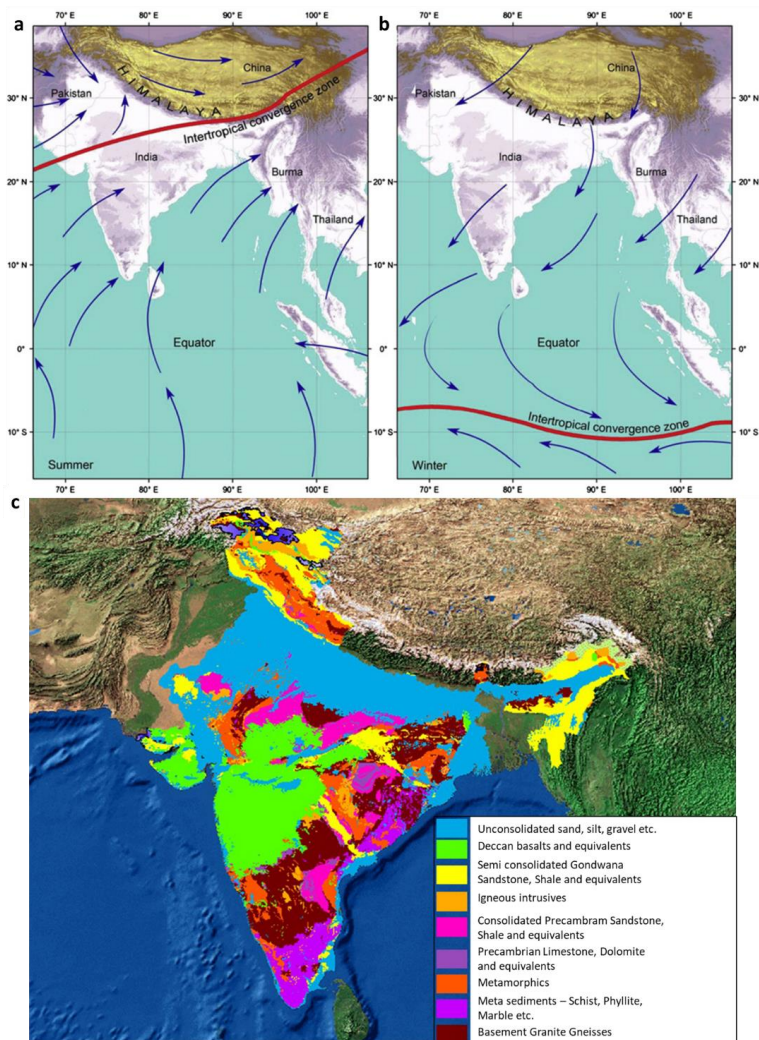
## 107 **2 Study region**

108 Peninsular India is a cratonic region with an approximate shape of a vast inverted triangle with diverse topography  
109 and characteristic climatic patterns, bounded by the Arabian Sea in the west, the Bay of Bengal in the east, and  
110 the Vindhya and Satpura ranges in the north. The long escarpments of the Western Ghats and the Eastern Ghats,  
111 constituting the western and eastern continental fringes of India, and an asymmetric relief with eastward tilt  
112 towards the floodplains of several eastward draining rivers from the 1.5 km high Western Ghats, characterize the  
113 physiography of Peninsular India (Richards et al., 2016).



114 The rise of the Himalayan-Tibetan plateau has significantly contributed to the Neogene climate of Asia, favoured  
115 the birth of the modern monsoon (Fig. 1.a, b) (Chatterjee et al., 2013, 2017), and triggered glaciation in the  
116 Northern region. A wide variety of plateaux, open valleys, bedrock gorges, mountain ranges, inselbergs and  
117 residual hills constitute the geomorphology of Peninsular India (Kale & Vaidyanadhan, 2014). The Peninsular  
118 landscape is dominated by Deccan Traps (Deccan basalts) of Cretaceous-Eocene, igneous and metamorphic rocks  
119 (Granite-gneisses) of Archaean-Late Precambrian along with minor consolidated sediments (Sandstone, shale) of  
120 Precambrian-Jurassic (Fig. 1.c) (Kale, 2014).

121 The region is strongly impacted by monsoons, major seasonal winds which are a manifestation of the seasonal  
122 movement of the Intertropical Convergence Zone (ICTZ in Fig. 1.a and Fig. 1.b), which contribute largely to the  
123 annual rainfall variability in much of the Indian subcontinent (Gadgil, 2003). The monsoons have two components  
124 – South-West monsoon and North-East monsoon, which arrive during June – September (JJAS) and October –  
125 December (OND), respectively. South-West monsoon season contributes more than 75% of annual rainfall over  
126 majority of the regions of the country (Saha et al., 1979). However, the Southern Peninsula receives a significant  
127 portion (30-60%) of its annual rainfall during the North-East monsoon, which contributes only 11% of the rainfall  
128 annually to India as a whole (Rajeevan et al., 2012). The maximum extent of rainfall over the Southern Peninsula  
129 during the North-East Monsoon is due to the reversal of lower-level winds over South Asia from the South-West  
130 to the North-East during the retreating phase of the South-West monsoon (Rajeevan et al., 2012). In Peninsular  
131 India, there is a spatial variability of the South-West monsoon in the south-north direction. For example, the  
132 Western Ghats, located at the western edges of Krishna and Cauvery basins, obstruct the incoming South-West  
133 monsoon winds causing heavy rainfall on the mountains. After crossing the Western Ghats, the monsoon winds  
134 have less moisture, causing a sharp decline in rainfall amounts towards the central and the north-eastern part of  
135 the Peninsula (Fig S2.a in Supplementary Material). The North-East monsoon occurs during winter, and mostly  
136 influence the rainfall in the Cauvery and some parts of the Krishna basins. Vegetation on the long escarpment of  
137 Western Ghats is primarily tropical evergreen forest, which plays an important role in intercepting the South-West  
138 monsoon winds (Ramachandra, 2018). Ramachandra (2018) portrayed the profile of vegetation across the west-  
139 east gradient as it varies from tropical-evergreen to semi-evergreen and then moist to dry deciduous forests  
140 towards the rain-shadow region just east of the Western Ghats. The topography map for the Peninsular region and  
141 a selected point in the region is depicted in Fig. S1.a and Fig. S1.b in Supplementary Material, respectively. The  
142 western margin of Peninsular India experiences heavy rainfall due to the presence of Western Ghats, whereas the  
143 rain shadow region witnesses deficient rainfall (Fig. S2.c). It can thus be seen that the long geological, tectonic  
144 history and the onset of monsoon climate events have made an imprint in the shaping the present landform of the  
145 Indian Peninsula (Kale, 2014).



146

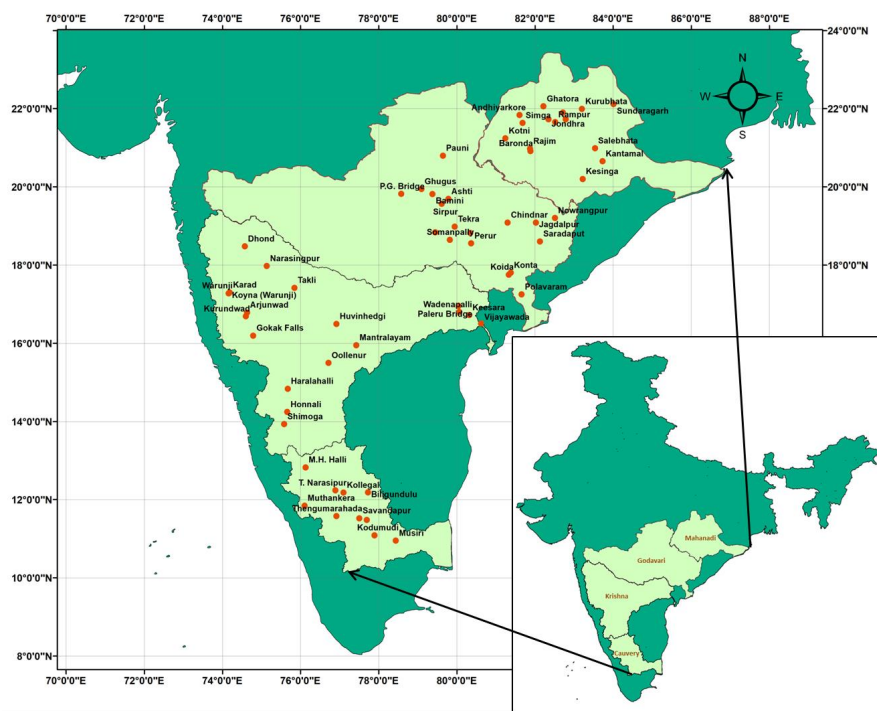
147

148 **Figure 1.** (a) The relation of uplift of Himalaya-Tibetan Plateau and monsoon initiation in India. Monsoon winds  
149 blow from the Indian Ocean towards land in the summer (b) during the winter, the Himalaya prevents cold air  
150 from passing into the subcontinent and causes the reversal of wind direction and monsoon blow from land toward  
151 sea [Reprinted from (Chatterjee et al., 2013)] (c) geology of Peninsular India [Reprinted from: Central Ground  
152 Water Board(<https://www.aims-cgwb.org/general-background.php>)].



153 The region shown in Fig. 2 is selected as the study area in the Deccan Plateau of Peninsular India. The escarpment  
154 of Western Ghats forms the western margin of the Deccan Plateau which serves as the main water divide for the  
155 Peninsular River systems. The gentle slope from west to east causes Peninsular rivers such as the Mahanadi,  
156 Godavari, Krishna, and Cauvery (Fig. 2) to flow eastwards. Three of these rivers (Godavari, Krishna and Cauvery)  
157 originate from the Western Ghats, spread across the area from the Deccan Plateau, flow eastwards, and drain into  
158 the Bay of Bengal. The Mahanadi River rises in the mountains of Siwaha bounded by the Eastern Ghats in the  
159 south and east, and drain eastwards into the Bay of Bengal. The Mahanadi basin constitutes a total catchment area  
160 of about 141,600 km<sup>2</sup> with an average annual rainfall of 1,360 mm and a mean annual river flow of 66,640 million  
161 m<sup>3</sup> (Rao et al., 2017). With an annual average rainfall of 1096 mm, the Godavari, the largest of all Peninsular  
162 rivers, receives nearly 84 percent of its annual rainfall on average during the South-West monsoon (Koneti et al.,  
163 2018). The Godavari basin's challenges include frequent flooding in its deltaic lower reaches, given the area's  
164 proximity to the coastal zone, which is prone to cyclones, and frequent drying up during the drier months (Koneti  
165 et al., 2018). Krishna is Peninsular India's second-largest river, with a total catchment area of 2,60,000 km<sup>2</sup>, and  
166 is susceptible to floods and droughts in some specific regions (Chanapathi & Thatikonda, 2020). The South-West  
167 monsoon is the most significant contributor to rainfall in the Krishna basin, accounting for about 90% of its total  
168 rainfall; the Krishna Basin, however, has a non-uniform rainfall distribution caused by climate variability, with  
169 an average annual rainfall bout of 770 mm (Chanapathi & Thatikonda, 2020). Annual rainfall in the Cauvery  
170 varies from 621 mm in the lower reaches to 4137 mm in the mountainous uplands, exhibiting considerable  
171 variation across the basin (Kumar Raju & Nandagiri, 2017). The river Krishna, with a mean annual runoff of less  
172 than 100 mm, is designated as an arid river (Milliman JD, 2011; Gupta et al., 2022), Cauvery as a semiarid river  
173 (100–250 mm), Mahanadi and Godavari as humid rivers (250–750 mm). The higher baseflow index occurs within  
174 0.5 and 0.7 in catchments in the Godavari and Mahanadi basins, whereas the lower baseflow index is noted from  
175 0.25 and 0.45 in the Cauvery and Krishna basins (Bhardwaj et al., 2020). For agricultural purposes, the semiarid  
176 regions of the Cauvery basin rely more on groundwater than surface water when compared to the other three  
177 basins (Sreelash et al., 2020).

178 In this study, daily streamflow data between 1965 to 2012 for 62 stream gauges (Fig. 2) are selected from Water  
179 Resources Information System database (WRIS) and located across the four river basins. The daily gridded rainfall  
180 product at spatial resolution of 0.25° × 0.25° from India Meteorological Department (IMD) is also employed for  
181 the analysis (Pai et al., 2014).



182

183 **Figure 2.** Location map of four Peninsular River Basins. Stream gauges considered in this study are marked with  
184 red circles.

185

### 186 3 Conceptual framework for stratification of streamflow variability using time scale

187 In this section, we check the suitability of a framework to stratify observed streamflow time series in the time  
188 domain into distinct time scales to better understand the physical controls of streamflow variability across the  
189 region. Partitioning of streamflow across seasonal and monthly time scales is able to bring out the role of climate  
190 seasonality on streamflow variability. Moreover, the progression of the seasons spatially imparts signatures on  
191 streamflow variability regionally as a whole. Time scale partitioning thus offers an opportunity to understand  
192 these climatic and landscape controls on streamflow variability through quantifying the relative contributions of  
193 seasonal streamflow on annual streamflow variability and how they vary regionally.

194 The streamflow hydrograph is the response of a physical, deterministic system (catchment) to a sequence of  
195 rainfall events. Given that the rainfall events are very much random in all their properties, equivalently, the  
196 streamflow hydrograph can also be seen as a stochastic time series, with streamflow considered a random variable.  
197 Therefore, it is amenable to a stochastic treatment in terms of distribution functions (e.g., cumulative distribution  
198 function, CDF). A major advantage of the CDF is that it enables us to make a concise statement of streamflow  
199 variability across a population of events. They have diagnostic value in that they can explain or interpret a  
200 catchment's streamflow response and compare it across many catchments and they help to classify catchments  
201 based on the flow regimes. They also have practical value in engineering design and environmental monitoring



202 that require a probabilistic treatment of streamflow. The cumulative distribution function of a random variable  
203 (the random variable of interest to us is daily streamflow;  $Q$ ) expresses the probability that a realization (i.e.,  
204 observation) of  $Q$  does not exceed a specific value  $q$ :

205 Cumulative Distribution Function (CDF):

$$F(q) = P[Q \leq q] \quad (1)$$

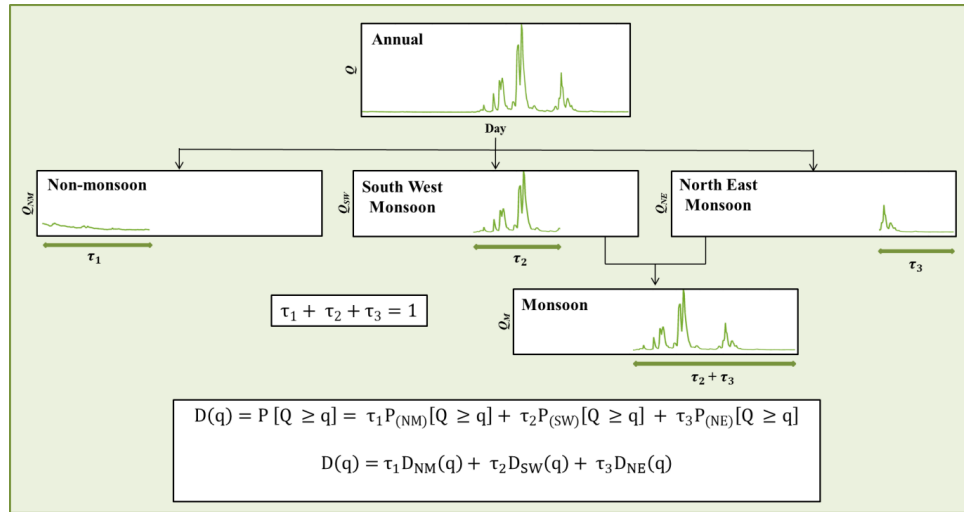
206 The flow duration curve is an alternative, but equivalent, measure of the streamflow variability that is widely used  
207 in hydrology. The flow duration curve is a plot that shows the fraction of time ( $D$ ) that the streamflow is likely to  
208 equal or exceed some specified value of interest. Mathematically,  $D$  can be expressed as,

$$D(q) = P[Q \geq q] = 1 - F(q) \quad (2)$$

209 Despite its probabilistic definition given above, in hydrological applications, the flow duration curve is plotted in  
210 terms of  $q(D)$  i.e.,  $q$  (in the vertical axis) as a function of  $D$  (in the horizontal axis).

#### 211 *Time scale partitioning of streamflow variability*

212 The streamflow time series can be equivalently divided into temporal segments of distinct seasons as well as  
213 distinct months. In this case, by joining observed time series over multiple years, FDCs for each time segment can  
214 be reconstructed. Assuming independence (as an approximation), these can then be combined to generate annual  
215 FDCs. The theory for the time scale partitioning is illustrated in Fig. 3. The year is divided into three distinct (non-  
216 overlapping) seasons, viz. Non-monsoon, South-West, and North-East seasons (for Peninsular India) of relative  
217 durations  $\tau_1$ ,  $\tau_2$ , and  $\tau_3$  (with  $\tau_1 + \tau_2 + \tau_3 = 1$ ) respectively. These seasons can be assumed to have distinct  
218 characteristics in terms of rainfall variability and how they translate to streamflow variability. The daily  
219 streamflow time series is used to construct the seasonal as well as annual FDCs. For example, the FDC of Non-  
220 monsoon season is constructed by using the daily streamflow during the period of January – May over the years.  
221 Similarly, FDCs for South-West and North-East monsoons are constructed using the daily streamflow during June  
222 – September and October – December months over the years respectively and the annual FDC is constructed using  
223 daily streamflow values for 365/366 days over the years. The FDCs at monthly time scales are obtained using the  
224 daily values of streamflow in a month over the years. The FDCs for the three distinct seasons, i.e., Non-monsoon,  
225 South-West monsoon, North-East monsoon, are denoted as  $D_{NM}(q)$ ,  $D_{SW}(q)$ , and  $D_{NE}(q)$  respectively. Initially,  
226 the FDCs for each season can be constructed separately (Fig. 3).



227

228 **Figure 3.** Scale partitioning into seasonal and monthly time scales. The conceptual framework illustrates the time  
 229 scale partitioning of streamflow time series into various seasonal components considering patterns of rainfall  
 230 variability. The annual streamflow time series is decomposed into three components: (1) Non-monsoon flow, (2)  
 231 South-West monsoon flow, and (3) North-East monsoon flow.

232

233 The annual FDC with exceedance probability  $P [Q \geq q]$  refers to the probability of flow in annual scale being  
 234 greater than or equal to  $q$ , and is expressed as

$$D(q) = P [Q \geq q] = \tau_1 P_{(NM)}[Q \geq q] + \tau_2 P_{(SW)}[Q \geq q] + \tau_3 P_{(NE)}[Q \geq q] \quad (3)$$

$$\text{or, } D(q) = \tau_1 D_{NM}(q) + \tau_2 D_{SW}(q) + \tau_3 D_{NE}(q) \quad (4)$$

235 where,  $P_{(NM)}[Q \geq q]$ ,  $P_{(SW)}[Q \geq q]$  and  $P_{(NE)}[Q \geq q]$  refer to, respectively, the probability of flow in Non-  
 236 monsoon, South-West monsoon and North-East monsoon being greater than  $q$ . As the seasons are non-  
 237 overlapping, the probability of flow being greater than  $q$  at annual scale (i.e.,  $P [Q \geq q]$ ) can be expressed as the  
 238 sum of the weighted probabilities of flow being greater than  $q$  in the three seasons.

239 In general, the FDC at the annual scale can be constructed as follows:

$$D(q) = \tau_1 D_1(q) + \tau_2 D_2(q) + \dots + \tau_n D_n(q) \quad (5)$$

240 where  $n$  is the number of distinct seasons considered for the analysis and,  $\tau_1 + \tau_2 + \dots + \tau_n = 1$ . The validity of  
 241 the above depends on the assumption that there is no carryover of flows from one season to the next season (which



242 is an approximation). In this study, the assumption of independence between flows across three seasons is checked  
 243 using multivariate Hoeffding's test (see details in Text S1 of Supplementary Information).

244 If  $F_A(\cdot)$ ,  $F_{NM}(\cdot)$ ,  $F_{SW}(\cdot)$  and  $F_{NE}(\cdot)$  represent cumulative distribution function of daily flows during annual, Non-  
 245 monsoon, South-West monsoon and North-East monsoon, respectively, then using equation (2), equation (6) can  
 246 be written as:

$$1 - F_A(q) = \tau_1[1 - F_{NM}(q)] + \tau_2[1 - F_{SW}(q)] + \tau_3[1 - F_{NE}(q)] \quad (6)$$

247 Differentiating the above equation with respect to  $q$ ,

$$f_A(q) = \tau_1 f_{NM}(q) + \tau_2 f_{SW}(q) + \tau_3 f_{NE}(q) \quad (7)$$

248 where  $f_A(\cdot)$ ,  $f_{NM}(\cdot)$ ,  $f_{SW}(\cdot)$  and  $f_{NE}(\cdot)$  represent probability density functions of annual, Non-monsoon, South-  
 249 West monsoon and North-East monsoon flows respectively.

250 If  $Q$ ,  $Q_{NM}$ ,  $Q_{SW}$  and  $Q_{NE}$  represent random variables comprising of daily streamflow at annual, Non-monsoon,  
 251 South-West monsoon and North-East monsoon time scales respectively, the expectation  $E(Q)$  and variance  $V(Q)$   
 252 of annual flow in terms of seasonal flows can be expressed as

$$E(Q) = \tau_1 E(Q_{NM}) + \tau_2 E(Q_{SW}) + \tau_3 E(Q_{NE}) \quad (8)$$

$$V(Q) = \tau_1 E(Q_{NM}^2) + \tau_2 E(Q_{SW}^2) + \tau_3 E(Q_{NE}^2) - (E(Q))^2 \quad (9)$$

253 The magnitudes of  $\tau_1$ ,  $\tau_2$  and  $\tau_3$  are  $\frac{5}{12}$ ,  $\frac{4}{12}$  and  $\frac{3}{12}$  based on the annual proportions of Non-monsoon, South-West  
 254 monsoon and North-East monsoon respectively.

255 The same concept can be continued by combining the flows in different months, in which case the way to combine  
 256 monthly FDCs into an annual FDC is given by:

$$D(q) = \frac{1}{12} \sum_{m=1}^{12} D_m(q) \quad (10)$$

257 where  $m = 1, \dots, 12$ .

258 If  $Q_m$  represents the random variable daily streamflow over  $m^{\text{th}}$  month, then the expectation  $E(Q)$  and variance  
 259  $V(Q)$  of annual flow in terms of monthly flows can be expressed as



$$E(Q) = \frac{1}{12} \sum_{m=1}^{12} E(Q_m) \quad (11)$$

$$V(Q) = \frac{1}{12} \sum_{m=1}^{12} E(Q_m^2) - (E(Q_A))^2 \quad (12)$$

260 The relative contributions of Non-monsoon ( $C_{NM \rightarrow AN}$ ), South-West monsoon ( $C_{SW \rightarrow AN}$ ) and North-East monsoon  
 261 ( $C_{NE \rightarrow AN}$ ) flows to annual flow can be approximated through following expressions:

$$C_{NM \rightarrow AN} = \frac{\tau_1 E(Q_{NM})}{\tau_1 E(Q_{NM}) + \tau_2 E(Q_{SW}) + \tau_3 E(Q_{NE})} \quad (13)$$

$$C_{SW \rightarrow AN} = \frac{\tau_2 E(Q_{SW})}{\tau_1 E(Q_{NM}) + \tau_2 E(Q_{SW}) + \tau_3 E(Q_{NE})} \quad (14)$$

$$C_{NE \rightarrow AN} = \frac{\tau_3 E(Q_{NE})}{\tau_1 E(Q_{NM}) + \tau_2 E(Q_{SW}) + \tau_3 E(Q_{NE})} \quad (15)$$

262 Similarly, the relative contributions of monthly flows to annual flow can be expressed as:

$$C_{m \rightarrow AN} = \frac{\frac{1}{12} E(Q_m)}{\frac{1}{12} \sum_{m=1}^{12} E(Q_m)} \quad (16)$$

263 where,  $m = 1, 2, \dots, 12$ , represents the index for months.

264 Note, as before, these relative contributions to total flow effectively also measure the relative contributions of the  
 265 seasonal/monthly flows to the mean of the annual flow duration curve.

266 The methodology for constructing annual FDC using seasonal FDC is as follows:

267 1. The empirical PDFs –  $f_{NM}(q)$ ,  $f_{SW}(q)$  and  $f_{NE}(q)$  are derived for daily streamflow time series for Non-  
 268 monsoon, South-West monsoon and North-East monsoon seasons respectively.

269 2. These PDFs are then multiplied by scaling factors,  $\tau_1$ ,  $\tau_2$  and  $\tau_3$  in equation 9. The scaling factors represent  
 270 relative durations of the three seasons considered. For example,  $\tau_1 = 5/12$ , as the duration of duration of non-  
 271 monsoon season is 5 months.

272 3. The PDF of annual flow is estimated as the weighted sum of three scaled density functions corresponding to  
 273 three seasons (see Eq. 7). The annual flow consists of the daily streamflow for Non-monsoon, South-West  
 274 monsoon and North-East monsoon seasons.

275 The performance of the time scale partitioning framework is assessed using the metric, root mean square error  
 276 (RMSE). The method of estimation of  $q_{sim}$  is shown in Fig. S3.



$$277 \quad RMSE = \sqrt{\frac{1}{n} \sum_{i=1}^n (q_{actual} - q_{sim})^2} \quad (17)$$

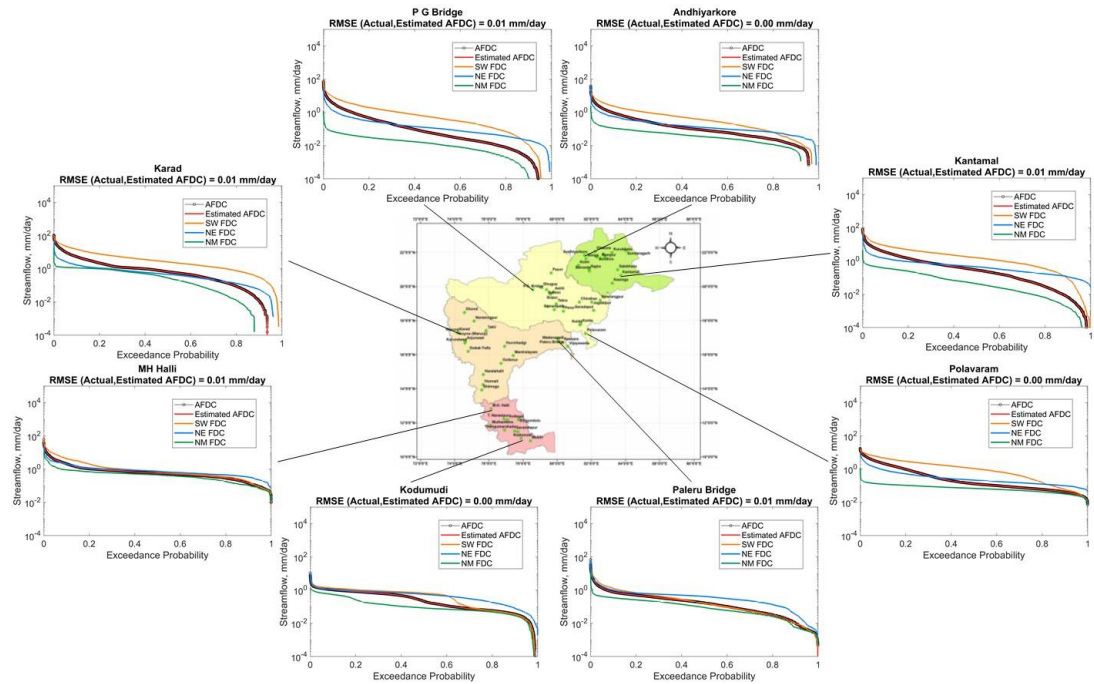
## 278 **4 Results**

### 279 **4.1 Time scale partitioning**

280 We initially investigated the spatial variations in seasonal and annual flow duration curves across Peninsular India  
281 employing the partitioning framework. The annual flow duration curve and seasonal flow duration curves for  
282 Non-monsoon, South-West monsoon, and North-East monsoon are shown in Fig. 4 for eight representative  
283 gauges, one at the upstream and one at the downstream of each of the four river basins. The estimated annual flow  
284 duration curve (red curve) using the equation 7 is also shown in Fig. 4. Daily streamflow time series is normalized  
285 by catchment area before plotting (on a semi-log paper) the flow duration curve for comparison across the gauging  
286 stations. In particular, the annual flow duration curve (black scatter) is reproduced well by the partitioning of both  
287 seasonal (red curve in Fig. 4) and monthly flows (red curve in Fig. S4). The mean and variance of annual flows  
288 are also reproduced well by the time scale partitioning framework (Fig. S5). This confirms the efficacy of the time  
289 scale partitioning approach of seasonal/monthly flows in approximating the annual flow duration curve (see also  
290 Fig. S4, Fig. S5.a and Fig. S5.d in Supplementary Material).

291 Another feature that can be observed in Fig. 4 is that in gauging stations located in the northern part of the  
292 peninsular region, flow duration curves (FDCs) of South-West monsoon flows (orange curve) are relatively higher  
293 than other seasonal FDCs. Given the logarithmic scale used to plot of the flows, this dominance is significant. In  
294 sites located in the southern part of the region, the dominance of South-West monsoon is not as strong and North-  
295 East monsoon flows (blue curve) are also significant.

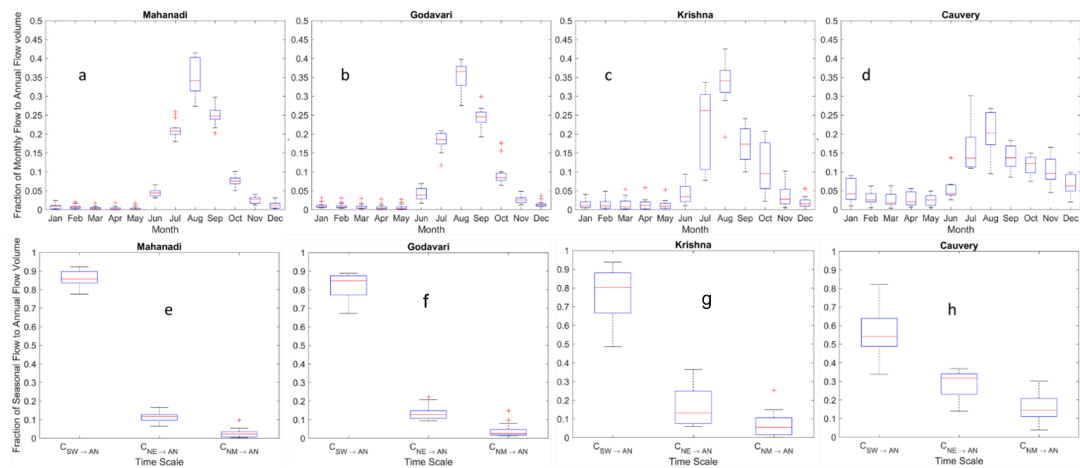
296 Motivated by these observations, we extracted seasonal and monthly streamflow time series from the entire dataset  
297 across all gauging stations to compute the relative contributions of seasonal and monthly flows to the annual flow  
298 duration curve. The results are presented in Fig. 5. At the monthly scale (top panel, Fig. 5), the contributions of  
299 flows during the months of June to September are much higher than in other months in northern Peninsular basins  
300 (Mahanadi and Godavari, Krishna to a less extent). This can be explained by the contribution of monthly rainfall  
301 to annual rainfall, which is higher during these months as shown in Fig. 6. On the other hand, in the southernmost  
302 Cauvery basin, the dominance of June to September months is relatively not as strong, and there is also a  
303 significant contribution during the months of October to December, higher than in northern basins (Fig. 5.d). This  
304 can be attributed to the slightly more equal dominance of both South-West (June - September) and North-East  
305 (October - December) monsoons over the Cauvery basin (Fig. 6.d) than in the northern basins. This pattern is also  
306 reflected at the seasonal scale (bottom panel, Fig. 5), with the contribution of South-West monsoon flow to annual  
307 flow being slightly higher than that during the other seasons, and much higher in northern basins. However, the  
308 contribution of South-West monsoon to annual flow decreases in southern basins, while the contribution of North-  
309 East monsoon increases, as can be seen clearly in Fig. 5.h for the Cauvery basin. The contribution of Non-monsoon  
310 to annual flow is also higher in southern basins relative to northern basins. This can be attributed to carry over  
311 flows from winter rains during the North-East monsoon, which is more pronounced in the southern part of the  
312 region.



313

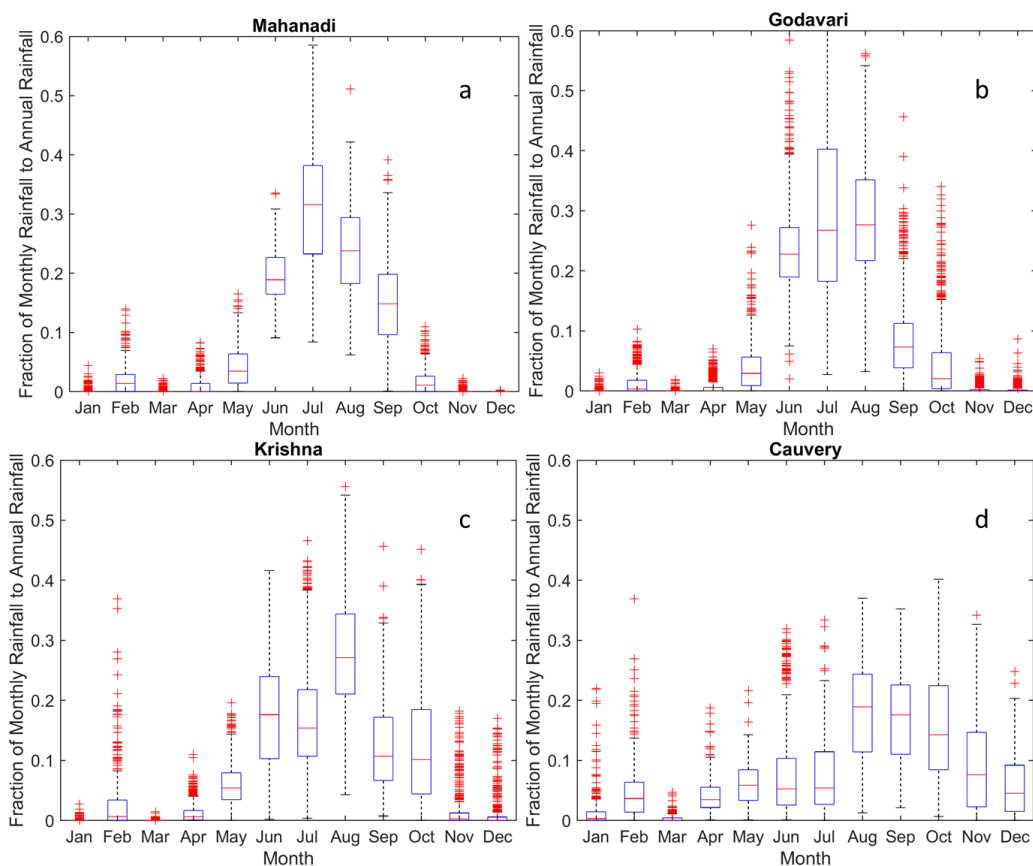
314 **Figure 4.** Spatial variations in seasonal and annual flow duration curves across Peninsular India. The time scale  
 315 partitioning framework of seasonal flows in approximating annual flow duration curves works reasonably well.

316



317

318 **Figure 5.** The relative contributions of monthly and seasonal flows to annual flow at basin scale. The contributions  
 319 of South-West monsoon flow to annual flow increases in northern basins whereas it decreases in southern basins.  
 320 However, the contributions of North-East monsoon flow to annual flow increases towards southern basins.



321

322 **Figure 6.** Long-term (1951-2010) fractional contribution of monthly rainfall across Peninsular  
323 basins.

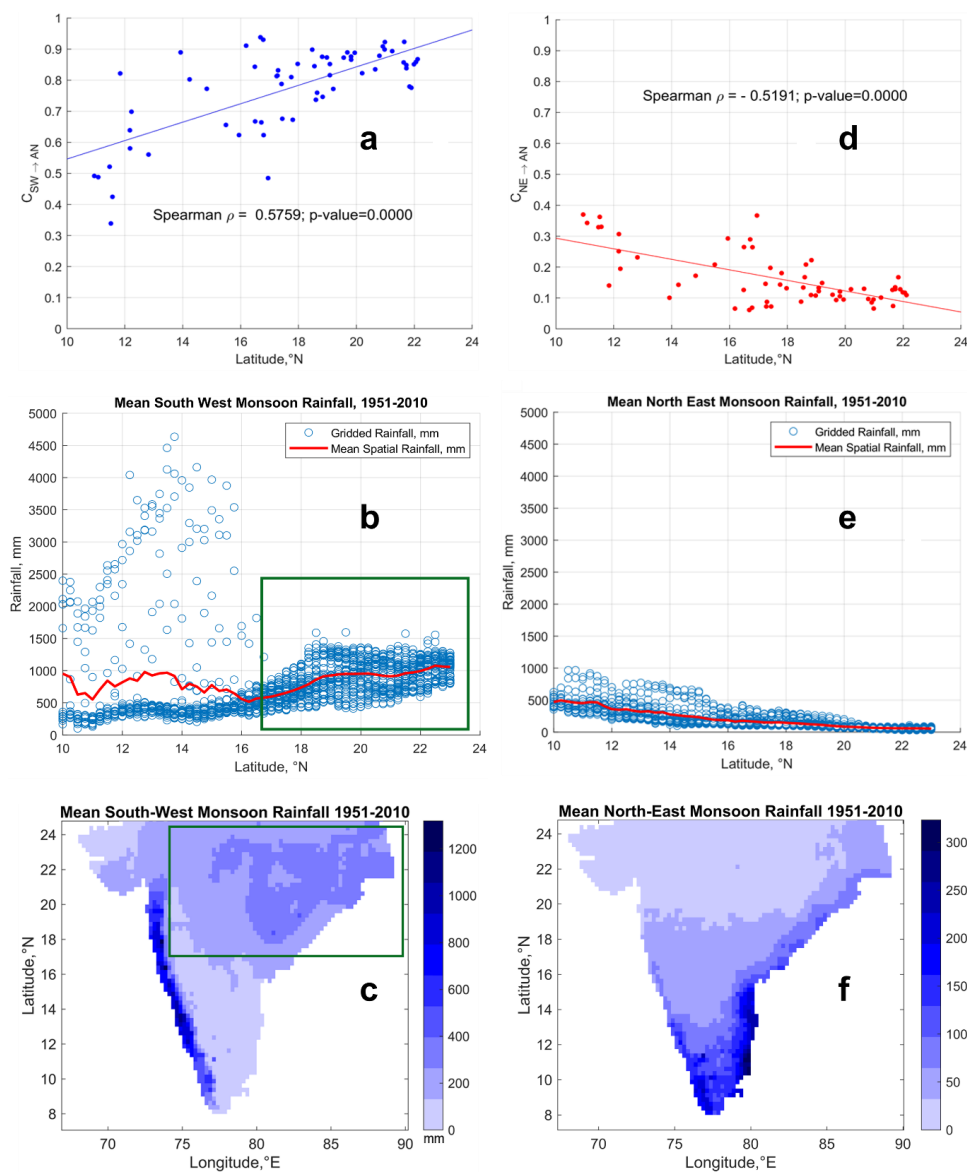


324 We next carried out regional scale analysis by considering streamflow time series of all the gauging stations across  
325 all four river basins. Similar to basin scale analysis presented before, the relative contributions of seasonal and  
326 monthly flows to annual flow are now estimated at the regional scale (Fig. 7). The spatial patterns of South-West  
327 and North-East monsoon rainfall across the Peninsular region are plotted for comparison using IMD gridded  
328 rainfall product (Fig. 7.b and Fig. 7.e).

329 The contribution of South-West monsoon flows to annual flow increases in the northerly direction (Fig. 7.a). The  
330 mountainous region of the southern Peninsula (western part of Krishna basin and north-western part of Cauvery  
331 basin) receives high rainfall during the South-West monsoon season (Fig. 7.b – extended till 17° N latitude). The  
332 streamflow produced in the headwater regions of southern basins in response to high rainfall, contributes at least  
333 70% of the annual flow (Fig. 7.a). Yet, the areal fraction of these high rainfall, headwater regions within the four  
334 river basins is quite small and their contributions to the average precipitation or flow at the basin scale is much  
335 smaller. There is also considerable variability in the contributions of South-West monsoon flows to annual flow  
336 in the sub-basins located at the eastern and south-eastern parts of Krishna and Cauvery basins (represented by the  
337 scatter below the regression line till 17° N latitude in Fig. 7.a) due to declining rainfall (Fig. 7c). This considerable  
338 variability, on average, reduces the overall contributions of South-West monsoon to annual flow in southern  
339 Peninsula with respect to the basins in the northern part.

340 The northern part of the Peninsular region receives comparatively higher rainfall than the southern part without  
341 considering the Western Ghats. This increased rainfall is attributed to the movement of low-pressure systems that  
342 develop over the Bay of Bengal towards central India (Krishnamurthy & Ajayamohan, 2010; Prakash et al., 2015).  
343 The low-pressure systems are a regular feature of South-West monsoon, which brings significant amount of  
344 rainfall in the northern part of the Peninsular region (Krishnamurthy & Ajayamohan, 2010). The increased rainfall  
345 (Fig. 7.b – after 16° N latitude) is responsible for higher contribution of South-West monsoon flows to annual  
346 flow in the northern basins. As the spatial variability of this rainfall is comparatively less than in the southern  
347 Peninsular region, there is less variability in the contribution of South-West monsoon flows to annual flow. The  
348 spatial variability in South-West monsoon along the south-north direction across Peninsular region can explain  
349 the gradient in the contribution of South-West monsoon flows to annual flow in the same direction.

350 On the other hand, the contribution of North-East monsoon flows to annual flow increases in the southerly  
351 direction (Fig. 7.d and Fig. 7.e). This can be explained by the fact that the southern part of the Peninsular region  
352 receives higher rainfall during North-East monsoon than the rest of the Peninsular region (Fig. 7.f).



353

354 **Figure 7.** Contribution of seasonal flows to annual flow at regional scale. The spatial variability of South-West  
 355 and North-East monsoons can explain the variation in contributions of seasonal flows to annual flow across south-  
 356 north gradient. The green box in (b) indicates the northern part of peninsular region which receives higher rainfall  
 357 than the southern part. The green box in (c) indicates the spatial extent of the rainfall grids which was considered  
 358 in figure (b). The red line in figure (b) indicates the mean rainfall – obtained by averaging the rainfall values at a  
 359 specific latitude (°N).



360 The application of the analysis framework used here is based on the critical assumption of independence of flows  
361 between different seasons (months), which needs to be critically evaluated. Moisture carry-over across seasons is  
362 a confounding issue in the case of strongly seasonal catchments (i.e., exhibiting sharp transition from wet season  
363 to dry season in terms of rainfall climatology), specifically when the initial wetness condition at the onset of the  
364 dry season depends on the final wetness at the end of wet season and vice-versa. Although most of the rainfall  
365 (58-90%) is concentrated during South-West monsoon months (i.e., June – September, red bar in Fig. S6) in  
366 Peninsular basins, more than 10% of the annual rainfall is received during North-East monsoon months (i.e.,  
367 October – December, yellow bar for Cauvery and Krishna in Fig. S6). In addition, more than 8% of annual rainfall  
368 occurs in non-monsoon season (i.e., January – May, blue bar in Fig. S6). This highlights that rainfall received  
369 during non-monsoon and North-East monsoon seasons are comparable, and thus it is difficult to distinguish the  
370 rainfall climatology across these seasons. Therefore, it is challenging to declare these are catchments with  
371 seasonally dry climates. In order to justify our assumption in the reconstruction of annual FDC from seasonal  
372 flows, we have now conducted a multivariate Hoeffding test (Gaißer et al., 2010) to check the independence  
373 between three random variables representing Non-monsoon, South-West Monsoon and North-East Monsoon  
374 flows respectively. A value of test statistic –  $\varphi^2$  – close to zero indicates independence between three random  
375 variables. It is observed that except for two stations in Krishna basin, 60 out of 62 stations show independence  
376 between flows across the seasons (Fig. S7). This supports appropriateness of the assumption of no carry-over that  
377 had been used in this study to construct annual FDC based on seasonal FDCs.

#### 378 **4.2 Combined influence of time scale and process scale partitioning**

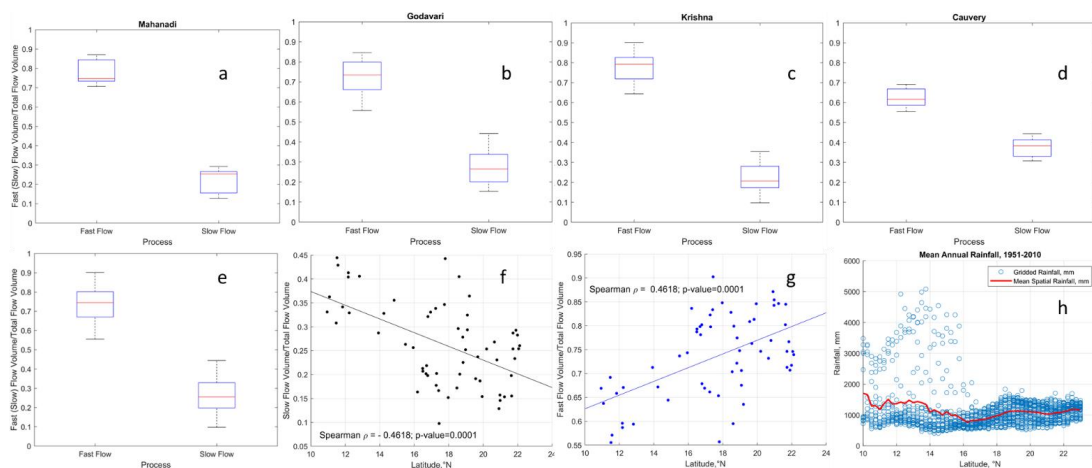
379 In order to further explore the climatic and landscape controls of streamflow variability regionally, we next  
380 partition streamflow into fast and slow flow components, notionally representing surface runoff, and a  
381 combination of subsurface and groundwater flow respectively (Ghotbi et al., 2020a, b) (see details in Text S2 and  
382 Fig. S8 in Supplementary Material). Fast flow is controlled by event scale runoff generation processes and its  
383 variability is characterized by topography, land use, soil and rainfall characteristics. On the other hand, climate  
384 seasonality and geologic formations of the subsurface are primary controllers of slow flow variability (Ghotbi et  
385 al., 2020a, b). The slow flow component is extracted from observed streamflow by using a recursive digital filter  
386 (see details in Appendix A.1). The fast flow component is obtained by then subtracting the slow flow from  
387 observed streamflow. The relative contributions of fast flow and slow flow to total flow (and hence also mean  
388 annual flow) are estimated using equations S2 and S3 respectively, for all the gauging stations across all four  
389 basins. The relative contributions of fast and slow flows to total flow at the basin and regional scales (combining  
390 all the gauging stations) are shown in Fig. 8. In addition, the long-term mean annual rainfall across the Peninsular  
391 region is also presented for comparison and to possibly explain the contributions of fast flow (Fig. 8.h).

392 The contributions of fast and slow flows to total flow in each of the four river basins is presented in Fig. 8.a to  
393 Fig. 8.d, indicating a strong dominance of fast flow in the northern basins (close to 80% in Mahanadi, Godavari  
394 and Krishna), and relatively less dominance (around 60%) in the southern Cauvery basin. This dominance of fast  
395 flow also shows up at the regional scale (Fig. 8.e). The regional variations of the relative contributions of slow  
396 and fast flows to total flow can also be seen in the results for individual gauges presented in Fig. 8.f and Fig. 8.g,  
397 respectively. On average, the contribution of slow flow decreases in the northerly direction, while the contribution  
398 of fast flow increases in a corresponding way.



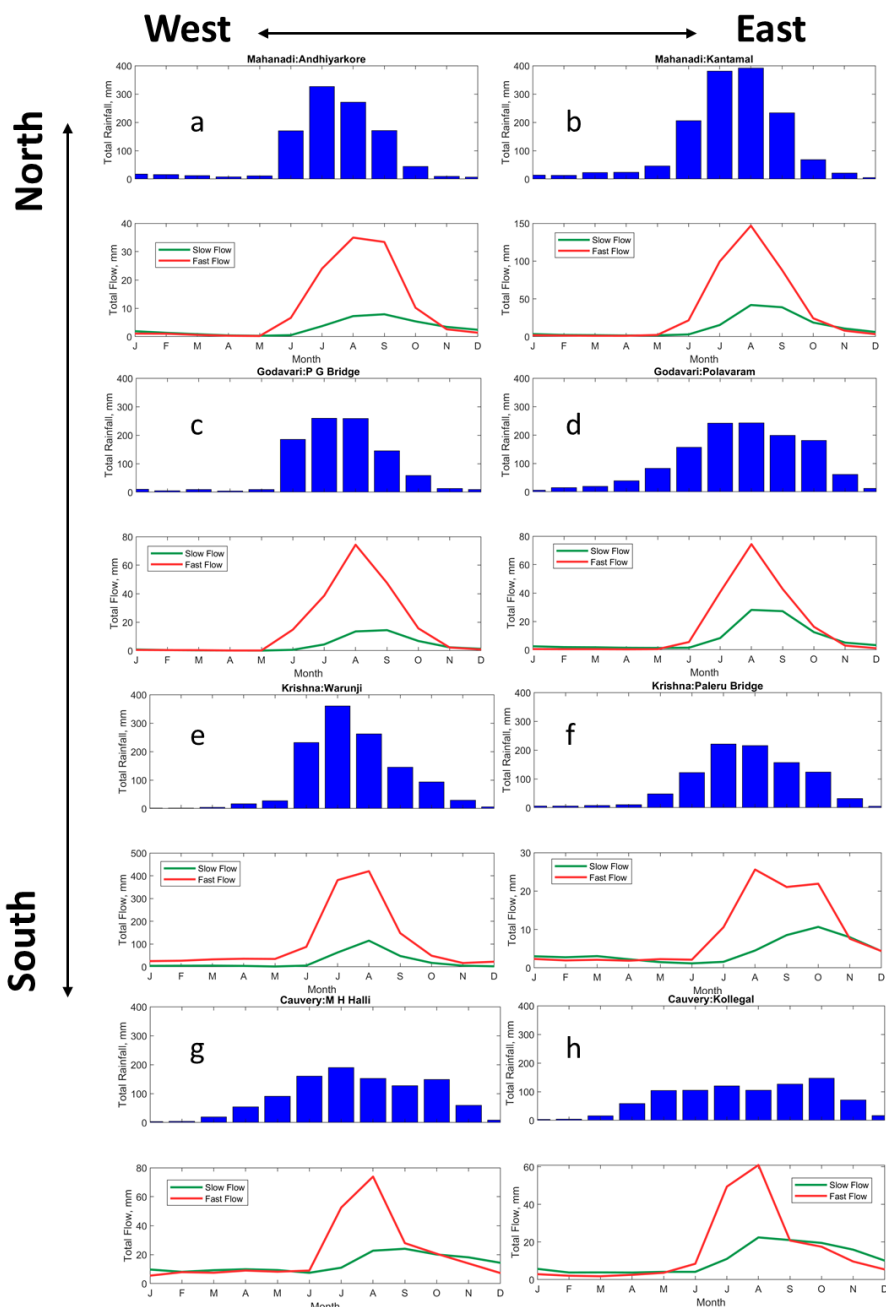
399 The contribution of fast flow to total flow increases in the northern direction of the Peninsular region (Fig. 8.g).  
400 The fast flow component of streamflow is generally more responsive to the characteristics of rainfall intensity.  
401 The southern part of the region receives high rainfall over Western Ghats along the western edge of Krishna basin  
402 and Cauvery basin (Fig. 8.h). In Cauvery basin, the headwater catchments (namely, MH Halli, Muthankera and  
403 Thengumarahada in Fig. 6) contribute 57 – 65 % of fast flow to total flow locally. The subbasins located at the  
404 western edges of Krishna basin contribute 80% of the fast flow to total flow (between 13° N and 18°N latitudes  
405 in Fig. 8.g) locally. However, there is a wide range of variability in the contributions of fast flow to total flow for  
406 subbasins located in the eastern part of Krishna basin. The spatial mean rainfall increases and variability decreases  
407 after 16° N latitude (Fig. 8.h), which dictate the increased contribution fast flow to total flow. Therefore, the  
408 spatial characteristics (mean and variability) of annual rainfall control the south-north gradient in fast flow  
409 contributions to total flow. In order to explain the variability in slow flow fraction of total flow, a multivariate  
410 regression analysis is performed (details are provided in Appendix, A.5). It is observed that the location of the  
411 gauges is an important predictor of the slow flow fraction of total flow in Peninsular region, revealing the existence  
412 of regional groundwater gradient in the region (Table A.1). In addition to the location of the gauges, the recession  
413 parameter,  $\beta$  – that controls the aquifer geometry and water level elevation profile during early and late stages of  
414 recession – is found to be significant in explaining the slow flow fraction of total flow (Table A.1).

415 The contributions of slow flow to total flow increases in the southerly direction over the Peninsular region (Fig.  
416 8.f). This can be explained by two major factors. Firstly, the Peninsular region is mostly dominated by hard rock  
417 geologic formations, where the subsurface flows are controlled by secondary porosities due to weathering and  
418 fracturing (Chandra, 2018; Das, 2019). The distribution of these formations is highly heterogenous (Fig. 1.c) and  
419 is responsible for baseflow (slow flow) contribution to total flow (Collins et al., 2020; Narasimhan, 2006). For  
420 example, 84% of the total area of Cauvery basin is classified as moderate and good groundwater potential zone  
421 (Arulbalaji et al., 2019). The influence of such potential regions of Cauvery basin is reflected on the presence of  
422 significant amount of slow flow even in the Non-monsoon season (Fig. 9.g and Fig. 9.h). Likewise, 63% of the  
423 total area of Krishna basin is classified under same category (Harini et al., 2018). However, the slow flow regime  
424 becomes much more seasonal (Fig. 9) in the northern part of the Peninsular region due to limited capability of  
425 geologic formations in transmitting slow flow (Patil et al., 2017) as well as strong seasonality in rainfall patterns  
426 (Fig. 9). Secondly, the southern part of the Peninsula receives rainfall almost equally during both South-West and  
427 North-East monsoons, which is reflected in the bimodal pattern of rainfall seasonality (Fig. 9.g and Fig. 9.h). The  
428 compounding effect of bimodal rainfall seasonality and higher fraction of moderate to good groundwater potential  
429 zones explains the higher contribution of slow flow to total flow in southern part of the Peninsular region.



430

431 **Figure 8.** Relative contributions of fast and slow flow to total flow. Consistent higher contribution of fast flow  
432 and lower contribution of slow flow to total flow are observed in Peninsular India (a – d) at basin scale. At regional  
433 scale, a systematic gradient in fast and slow flow contributions is observed (f and g). The spatial patterns of rainfall  
434 (h) can explain the gradient in fast flow contributions. The high scatter of rainfall in the low latitudes represents  
435 the heavy rainfall with high variability occurring in the Western Ghats.



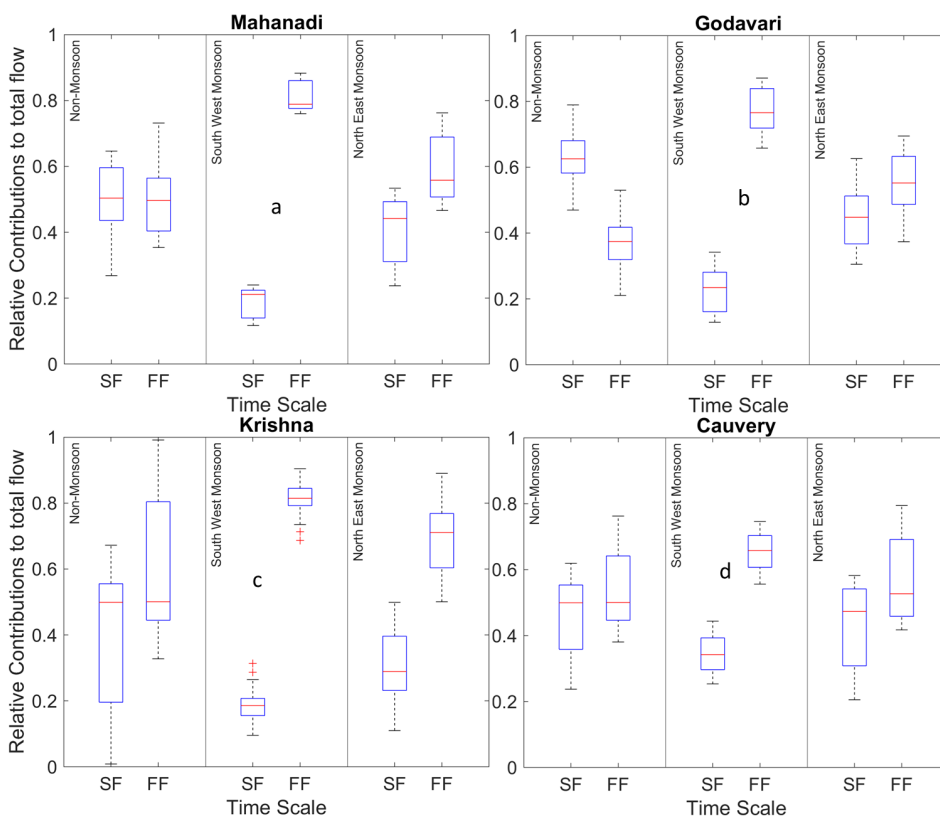
436

437 **Figure 9.** Spatial variation of long-term monthly fast and slow flow components of streamflow at selected gauges  
 438 in Peninsular region. The blue bar plots represent the long-term monthly rainfall averaged over the sub-basins  
 439 corresponding to the gauging stations. The seasonality in rainfall patterns changes (unimodal to bimodal) across  
 440 north-south direction of the Peninsular region.



441 Further, an investigation of the combined influence of climatic time scales and process time scales is therefore  
442 pertinent to fully understand the controls of streamflow variability in this region. To address this question, we  
443 extracted the fast and slow flow components for each of the Non-monsoon, South-West monsoon and North-East  
444 monsoon seasons. These components are then used to estimate their relative contributions to total flow for the  
445 three seasons across all the gauging stations.

446 The relative contributions of fast and slow flow to total flow at basin scale are shown in Fig. 10. It is observed  
447 that during the Non-monsoon period, the median contributions of fast and slow flow for Mahanadi, Krishna and  
448 Cauvery basins are similar, although there exists considerable variability in their distribution. With the onset of  
449 the South-West monsoon, the contribution of fast flow to total flow increases markedly for all the basins, although  
450 relatively much less in the Cauvery basin. During the subsequent North-East monsoon season, the contribution of  
451 fast flow decreases whereas slow flow contribution increases. The fluctuations in the fast flow contributions can  
452 be explained by the onset and withdrawal of the monsoon seasons, which are major contributors to fast flow  
453 generation. The fluctuations in the fast flow contributions across seasons can be explained by the differences in  
454 the rainfall amount during South-West and North-East monsoons (Fig. 7.c and Fig. 7.f). Among all four basins,  
455 the difference in median contributions of fast and slow flow is minimum. These can be attributed to the presence  
456 of higher fraction of moderate and good groundwater potential zones (Arulbalaji et al., 2019) which promotes  
457 baseflow even in dry periods (Fig. 9.g and Fig. 9.h). The presence of bimodal pattern in rainfall seasonality due  
458 to both South-West and North-East monsoons minimizes the difference between the relative contributions of fast  
459 and slow flow to total flow.



460

461 **Figure 10.** Seasonal contributions of fast (FF) and slow flow (SF) to total flow at basin scale.

462

## 463 5. Validation of stratification of streamflow variability

### 464 5.1 Understanding physical controls and spatial variation of flow duration curve by fitting statistical 465 distributions

466 So far in this paper, in order to understand the physical controls on regional streamflow variability across  
467 Peninsular India we have partitioned observed streamflows in two ways: (i) seasonal/monthly flows, and (ii) slow  
468 and fast flows. We looked at the relative contributions of these components to mean annual streamflow, looked at  
469 how the relative contributions varied regionally, and attributed these to the relative strengths of the monsoons and  
470 spatial variations of geological formations. We now return to the FDCs of the flow components, especially the  
471 shapes of the FDCs (as reflected in the parameters of the fitted distribution) and look at how they themselves vary  
472 regionally.

473 In our study the fast and slow flow time series are scaled by their respective long-term mean values to remove the  
474 influence of mean climate and geology, thus providing an opportunity to identify the secondary controls on the  
475 variation of shapes of FDCs. The scaled fast and slow flow time series are now used to fit the mixed gamma  
476 distribution (MGD, (see details in Appendix A4). The parameters of mixed gamma distribution control the shape

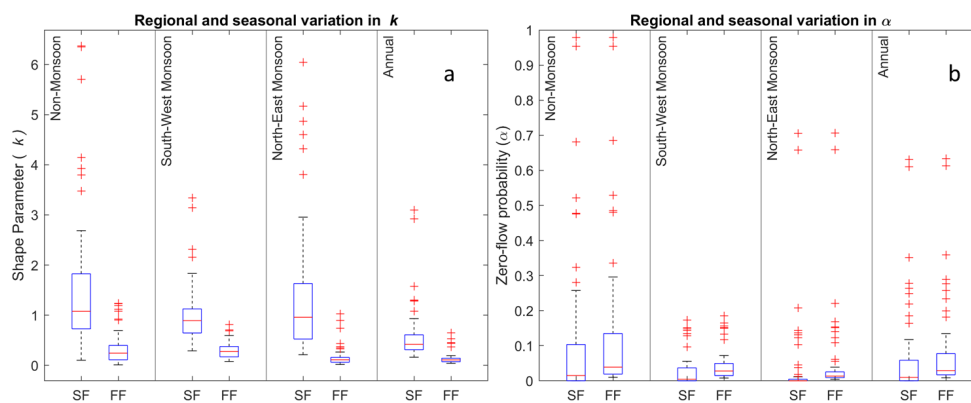


477 and orientation of the FDC. For example, the shape parameter  $k$  controls the slope of the FDC whereas  $\alpha$  controls  
478 the zero-flow part of the FDC. However, the parameter  $\theta$  affects the vertical shift of the FDC. In addition, these  
479 parameters are also linked with the mean and variance of the streamflow time series. For example, the scale  
480 parameter  $\theta$  is directly proportional to the mean of the time series whereas, the shape parameter  $k$  is inversely  
481 proportional to the variance of the time series.

482 As the fast and slow flow time series are scaled with their respective long-term means, the scale parameter ( $\theta$ ) is  
483 approximately found to be inversely proportional to shape parameter ( $k$ ) through the relationship,  $k\theta = \frac{1}{1-\alpha}$   
484 (Cheng et al., 2012). Therefore, the variations of only  $k$  and  $\alpha$  – zero-flow probability, are presented in this section.  
485 The variation of  $k$  can be related to the steepness of the FDC, i.e., smaller values of  $k$  will have steeper slopes.

486 The Nash-Sutcliffe efficiency (NS) and coefficient of determination ( $R^2$ ) goodness of fit of fast/slow flows to  
487 MGD is shown in Fig. S10 (in Supplementary Information). In addition, the observed and simulated fast and slow  
488 flow FDCs are compared in Fig. S8 (in Supplementary Information). It is observed that the slow flow component  
489 fits well to mixed gamma distribution than fast flow component, as slow flow is most stable component and MGD  
490 satisfactorily captured the shape of slow flow FDC. However, MGD adequately captures the shape of fast flow  
491 FDCs at upper tail (high flow segment), except for the lower tail (low flow segment). The fast flow processes are  
492 governed by more complex processes (for example, infiltration and saturation excess runoff generation, runoff  
493 routing, stochastic nature of storm events, properties of soil and topography etc.) than slow flow (for example,  
494 climate seasonality and underlying geology of aquifer system).

495 The seasonal variation of parameters of the mixed gamma distribution at regional scale (comprising of all the  
496 gauging stations) is presented in Fig. 11. The mixed gamma distribution performed well in fitting the flow duration  
497 curves of two flow components across different seasons (Fig. S10). In Fig. 11.a, it is observed that the shape  
498 parameter of slow flow is consistently higher than that of fast flow. The shape parameter is inversely proportional  
499 to the variance of streamflow. The slow flow exhibits lower variance due to its longer time of residence in the  
500 subsurface formations. Moreover, the subsurface formations in Cauvery River basin are more favourable to slow  
501 flow in comparison to the other three basins (Fig. 9.g and Fig. 9.h). In addition, the bimodal seasonal pattern of  
502 rainfall is also responsible for occurrence of slow flow even in the Non-monsoon period for the southern basins  
503 (Fig. 9).



504

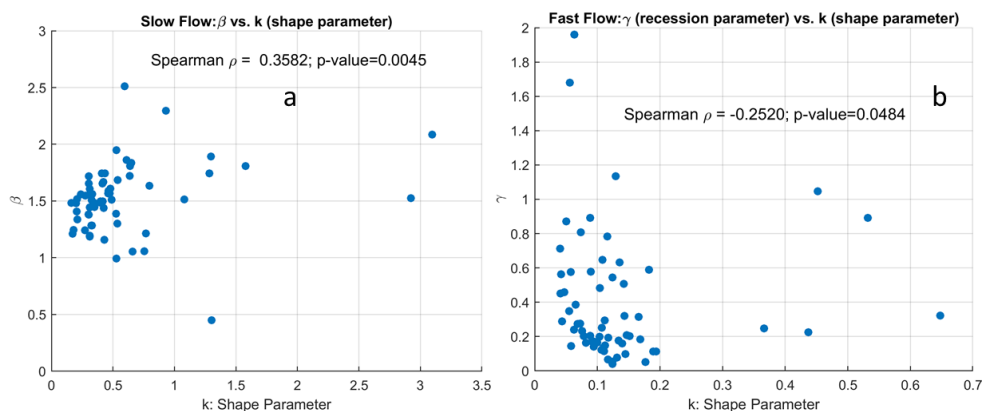
505 **Figure 11.** Regional and seasonal variation of  $k$  and  $\alpha$  parameter of mixed gamma distribution.

506 The fast flow component exhibits higher variance than the slow flow component. The median shape parameter of  
507 fast flow is highest during South-West monsoon season and lowest during North-East monsoon (Fig. 11.a). This  
508 can be explained by the lower variance of fast flow during South-West monsoon as the rainfall amount is higher  
509 during the season compared to the North-East monsoon (Fig. 7.c and Fig. 7.f). The dominance of both South-  
510 West and North-East monsoons in Cauvery basin results in lower variance of fast flow compared to the northern  
511 basins. The fast flow duration curves are steeper than the slow flow duration curves for all seasons, as the  
512 magnitudes of  $k$  for fast flow are smaller than that of slow flow (Fig. 11.a).

513 The parameter  $\alpha$  controls the zero-flow part of the flow duration curve. It is observed that the mean  $\alpha$  for slow  
514 flow is minimum during South-West monsoon and maximum for Non-monsoon season (Fig. 11.b) on a regional  
515 scale. This can be attributed to the combined influence of rainfall during South-West monsoon and the  
516 connectivity between underlying geologic formations in the Peninsular region. For the fast flow, the mean  $\alpha$  is  
517 minimum during the South-West monsoon and maximum during Non-monsoon as the South-West monsoon is  
518 the dominating rainfall season in Peninsular India.

519 The shape parameters ( $k$ ) of MGD for slow and fast flow components are linked with landscape properties through  
520 recession analysis, where the parameters  $\gamma$  &  $\beta$  of power-law relationship are estimated using streamflow data  
521 (details in Appendix A.2). It is observed that shape parameter (inversely proportional to variability) of slow flow  
522 is positively correlated with  $\beta$ . The parameter  $\beta$  is influenced by aquifer geometry and water table elevation  
523 profile defining early and late stages of recession (Tashie et al., 2020a; Tashie et al., 2020b). Higher values of  $\beta$   
524 indicate slow late recessions which is characterized by low variability in slow flow (Fig. 12.a).

525 The shape parameter of fast flow is negatively correlated with the parameter  $\gamma$  of the power-law relationship (Fig.  
526 12.b). The parameter  $\gamma$  strongly related with the seasonality of catchment wetness and evapotranspiration which  
527 are primary governing factors for runoff generation (Dralle et al., 2015; Gnann et al., 2021). In addition, the spatial  
528 variation of rainfall also influences the variability of  $\gamma$  (Biswal & Kumar, 2014) which reflects the variability of  
529 fast flow.

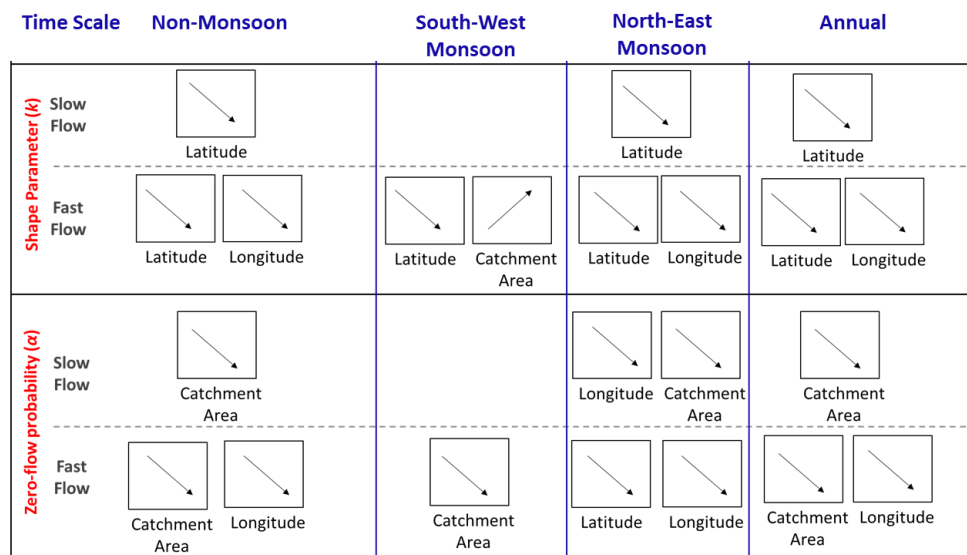


530

531 **Figure 12.** Relationship between flow variability (related inversely to shape parameter,  $k$  of mixed gamma  
532 distribution) and recession parameters.

533 The variation of the parameters,  $k$  and  $\alpha$  was also studied using spatial descriptors (latitude and longitude) as  
534 explanatory variables to understand the spatial variation of FDCs across south-north, west-east gradients. In  
535 addition, the behaviour of these parameters is also assessed using catchment area as another explanatory variable.  
536 The regional parameter sets comprising of  $k$  and  $\alpha$  are next constructed for slow and fast flow processes by  
537 including these parameters for all the time series across different gauging stations across the Peninsular region.  
538 The Spearman correlation coefficients between these parameters and explanatory variables (i.e., catchment area  
539 and spatial descriptors – latitude and longitude) for slow and fast flow processes at seasonal scales are computed.  
540 The schematic representation of significant directions (positive/negative correlations) in Spearman coefficient is  
541 shown in Fig. 13.

542



543

544 **Figure 13.** Schematic representation of spatial and temporal variation of parameters of mixed gamma distribution  
 545 across Peninsular India. The direction of significant Spearman correlation coefficient between model parameters  
 546 and descriptors (catchment area and spatial descriptors – latitude and longitude) for fast and slow flow across  
 547 multiple time scale is presented.

548 The shape parameter of fast flow is found to be positively correlated with catchment area (Fig. 13, top panel),  
 549 implying lower variability of fast flow in large catchments. This can be attributed to increased smoothing effect  
 550 of incoming rainfall in larger catchments through various storages, thus reducing the variability of fast flow.  
 551 Moreover, the shape parameters for fast flow are negatively correlated with spatial descriptors, indicating  
 552 increased variability of fast flow along south-north and west-east gradients. This can be partly explained by the  
 553 bimodal seasonal pattern of rainfall due to dominance of South-West and North-East monsoons, thus reducing the  
 554 variability of fast flow in the southern part of the region. The rainfall pattern becomes more seasonal (primarily  
 555 due to South-West monsoon) in the northern part of region which can contribute to increased variability of fast  
 556 flow. The presence of numerous water retention structures for supporting irrigation in these regions (54 – 75% of  
 557 Peninsular basins are crop land) can modify the variability of the flow, although we have not analysed this  
 558 separately in this study.

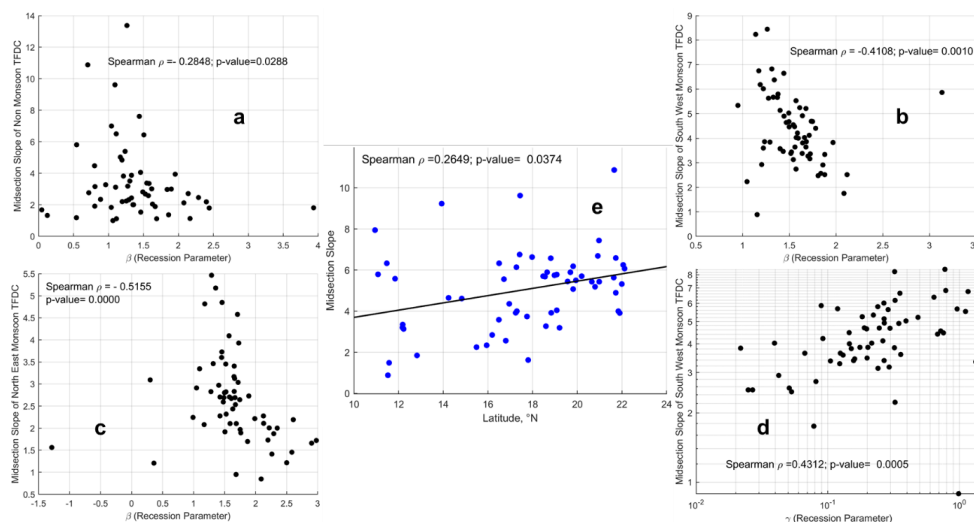
559 The shape parameter of slow flow is found to be negatively correlated with latitude, implying that slow flow  
 560 becomes highly variable in the northern part of the region. This can be explained by the nature of geologic  
 561 formations in the Cauvery basin that promotes slow flow even during the Non-monsoon period. However, in the  
 562 northern part of the region, the slow flow tends to become more seasonal and has very limited flow during non-  
 563 rainy seasons. In addition to the geology, the bimodal seasonal rainfall patterns due to monsoons can play an  
 564 important role in the variability of slow flow. Apart from the spatial descriptors, the slow flow variability is  
 565 inversely proportional to catchment area, implying larger catchments have lower slow flow variability than  
 566 smaller catchments. This can be explained by the proportional increase in area of contribution to slow flow with  
 567 increase in catchment size, thus reducing the variability in slow flow for larger catchments.



568 The parameter  $\alpha$  is found to be negatively correlated with catchment area (Fig. 13, bottom panel) for fast and slow  
 569 processes, implying zero-flow probabilities are lower for larger catchments. The higher residence time of water  
 570 in larger catchment due to various kinds of storages facilitates flow in river even in Non-monsoon season, thus  
 571 reducing the zero-flow probabilities. In addition, the parameter  $\alpha$  of both slow and fast flow are negatively  
 572 correlated with longitude, implying lower zero-flow probabilities along west-east direction. This can be attributed  
 573 to natural declining elevation (Fig. S1.b) which promotes both fast and slow flow towards eastern direction.

574 **5.2 Understanding physical controls and spatial variation of seasonal flow duration curve using mid-section**  
 575 **slope**

576 Apart from mean, variance and no-flow frequency, the midsection slope of the FDC – estimated using  
 577  $\frac{\ln(Q_{33p}) - \ln(Q_{66p})}{0.66 - 0.33}$ , where  $Q_{33p}$  and  $Q_{66p}$  represent the streamflow values at 33<sup>rd</sup> and 66<sup>th</sup> percentiles respectively –  
 578 is connected to the average flow regime of the catchment, which is controlled by both surface and subsurface  
 579 processes (Yokoo & Sivapalan, 2011; Chouaib et al., 2018). The association of the slope of FDC with the  
 580 parameters pertaining to recession analysis is presented in Fig. 14.



581

582 **Figure 14.** Association between streamflow variability and recession parameters.

583 During Non-monsoon and North East monsoon seasons (Fig. 14a and Fig. 14c) – when rainfall is comparatively  
 584 less than South West monsoon – a significant association between flow variability and  $\beta$  highlights the importance  
 585 of slow flow and recession characteristics controlled by aquifer geometry and water table elevation profile. In  
 586 addition to significant association with  $\beta$  during South West monsoon (Fig. 14b), the midsection slope of FDC is  
 587 positively correlated with  $\gamma$  – the parameter which is strongly related with the seasonality of catchment wetness,  
 588 evapotranspiration and spatial variation in rainfall – revealing the importance of land surface processes in  
 589 variability of streamflow variability.



590 A coherent pattern in variability of streamflow (via. Midsection slope of FDC) is observed across South – North  
591 gradient of the Peninsular region (Fig. 14e). This systematic pattern in streamflow variability reflects the influence  
592 of combined functioning of subsurface and land surface processes on regional hydrologic signatures of Peninsular  
593 India.

## 594 6. Conclusions

595 Being a signature of a catchment's hydrological behavior and a concise graphical summary of streamflow  
596 variability at a specific gauging station, FDC relates the frequency and magnitude of observed streamflows and  
597 helps explain flooding mechanisms and low flow conditions at the referred location. Furthermore, at the catchment  
598 scale, FDCs incorporate the forcing mechanisms of the water cycle and the physical and morphological properties  
599 of the river basin that influence the water partition between surface runoff and baseflow and, thus, control flow  
600 regimes (Costa & Fernandes, 2021). Motivated by this fact, in this study we outlined a framework and its  
601 suitability for understanding process controls of FDCs, which involved separating annual streamflow into seasonal  
602 flow components and constructing annual FDC using seasonal FDCs. The goal of this study was to demonstrate  
603 the efficacy of the framework to explore the process controls on streamflow variability across Peninsular India.  
604 The study followed a data-based approach using streamflow data taken from 62 stream gauges distributed within  
605 four major river basins in Peninsular India. The probability density functions are initially derived for daily  
606 streamflow time series for Non-monsoon, South-West monsoon, and North-East monsoon seasons. These PDFs  
607 are then multiplied by scaling factors that represent relative durations of the seasons considered. The probability  
608 density function of annual flow is then estimated as the weighted sum of three scaled density functions  
609 corresponding to three seasons. The performance of the time scale partitioning framework is then further assessed  
610 using the metric root mean square error.

611 Analysis and interpretation of the results of the study revealed that the main drivers of regional variability of  
612 streamflow across Peninsular India include (1) major mountain ranges – the Western and Eastern Ghats – which  
613 govern regional atmospheric circulation and precipitation variability; (2) the South-West and North-East  
614 monsoons that occur in different times of the year and come from different directions; and (3) east-west and north-  
615 south gradients of geology. The combined influence of seasonal rainfall patterns, catchment size and the ability  
616 of the subsurface formations to transmit slow flow controls the shape of flow duration curves of the flow  
617 components along south-north and west-east directions in Peninsular region.

618 To summarize, the major findings of the study are outlined below:

619 I. Spatial variations of seasonal and annual flow duration curves across Peninsular India are initially  
620 investigated by approximating the annual flow duration curve via partitioned seasonal and monthly flow  
621 duration curves. FDCs of South-West monsoon flows are relatively dominant to other seasonal FDCs at  
622 stations in the northern portion of the peninsula. From June to September, flow contributions in northern  
623 Peninsular basins are significantly higher than in other months (Mahanadi and Godavari, Krishna to a  
624 lesser extent). However, the contribution from June to September is not as substantial in the southernmost  
625 Cauvery basin; there is also a major contribution from October to December. This is attributable to the  
626 fact that the South-West and North-East monsoons both impact the Cauvery basin. It is further noticed  
627 that the contribution of the North-East monsoon to annual flow is larger in southern basins than in



628 northern basins. The contribution of the Non-monsoon to annual flow is also stronger in the southern  
629 basin and is attributed to winter rains from the North-East monsoon, which are more evident in the  
630 southern part of the peninsula, creating carryover flows.

631 II. The streamflow produced in the headwater regions of southern basins, which extends until 17° N latitude  
632 and contributes at least 70% of the annual flow, is a result of high rainfall during the South-West monsoon  
633 season in the mountainous region of the southern Peninsula (western part of Krishna basin and north-  
634 western part of Cauvery basin). The northern part of the Peninsular region experiences notably higher  
635 rainfall than the southern part, not considering the Western Ghats region. The low-pressure system, which  
636 is a regular feature of the South-West monsoon that brings significant rainfall in the northern part of the  
637 Peninsular region, attributes the increased rainfall (after 16° N latitude) and is responsible for the higher  
638 contribution of South-West monsoon flows to annual flow in the northern basins. The spatial variation in  
639 the contribution of South-West monsoon flows to annual flow in the south-north direction is thus  
640 explained by the spatial variability of the South-West monsoon in the same direction over the Peninsular  
641 region. The contribution of North-East monsoon flows to annual flow, on the other hand, increases in a  
642 southerly direction, which can be explained by the fact that the southern part of the Peninsular region  
643 receives more rainfall during the North-East monsoon than the rest of the Peninsular region.

644 III. Spatial variations of fast/slow and total flow duration curves across Peninsular India are then explored  
645 by approximating the total flow duration curve by partitioned flow duration curves. Relative  
646 contributions of fast and slow flows to total flow in each of the four river basins show a significant  
647 dominance of fast flow in the northern basins, close to 80% in Mahanadi, Godavari, and Krishna river  
648 basins.

649 IV. The Western Ghats, which run along the western boundary of the Krishna and Cauvery basins, bring a  
650 lot of rain to the southern part of the region. As a result, the western margins of the sub-basins along the  
651 Krishna basin contribute 80 percent of the fast flow to total flow (between 13° N and 18°N latitudes).  
652 However, the south-north gradient in fast flow contributions to total flow is governed by increasing  
653 spatial mean characteristics of annual rainfall after 16° N latitude, which dictates an increased  
654 contribution of fast flow to total flow.

655 V. The greater contribution of slow flow to total flow in the southern Peninsular region, particularly Cauvery  
656 and Krishna, is characterized by bimodal rainfall seasonality and the presence of a higher fraction of  
657 moderate to good groundwater potential zones and is responsible for the spatial variation of  
658 increased relative contributions of slow flow to total flow in the southerly direction over the Peninsular  
659 region.

660 VI. A coherent pattern in streamflow variability across the South-North gradient of the Peninsular region is  
661 observed via the midsection slope of FDC. These similar spatial variation in streamflow variability  
662 demonstrate the impact of combined subsurface and land surface processes on Peninsular India's regional  
663 hydrologic signatures.

664 Previous data-based explorations of process controls on the FDC have typically followed a Darwinian (Harman  
665 and Troch, 2014) comparative hydrology approach. They have looked at between-catchment and regional  
666 variations of the FDC (or of parameters of statistical distributions fitted to empirical FDCs), their attribution to  
667 climatic and landscape properties, and their interpretation in terms of their underlying process controls (fast flow



668 and slow flow etc). In the Darwinian approach, each catchment is deemed a particular but statistically independent  
669 realization of the coevolution of climate and landscape properties, with the hydrologic response being both a cause  
670 and effect in this coevolution (Wagener et al., 2013). The novelty of the data-based exploration of process controls  
671 on the FDC adopted in this study is that here we have followed a Wegenerian (cf. Alfred Wegener, Sivapalan,  
672 2018) comparative hydrology approach, in which the focus was on exploration of the controls of common regional  
673 landscape features (in space) and seasonal climatic variations (in time) features on regional variations of the FDC.  
674 We interpret the imprints of the regional variations streamflow variability of the FDCs outlined as findings across  
675 Peninsular India as the consequence of several episodes of tectonic, geological, and volcanic activities in the  
676 Indian subcontinent ever since the breakup of Gondwana and its collision with Asia during the Jurassic age,  
677 resulting in the uplift of mountain ranges, including the Himalayas, and their role in the establishment of India's  
678 monsoon climate.

679 We acknowledge, however, that in recent times streamflow variability in Peninsular India has been significantly  
680 impacted by anthropogenic activities, including significant land use and land cover changes, and other human  
681 interferences such as the building of dams and the extraction of water from both rivers and from groundwater  
682 aquifers for human use. The present study has not explored the effects of human impacts: their impacts on both  
683 temporal (inter-decadal) and spatial (regional) variations of the FDCs is left for future work. Further work is also  
684 needed to understand in more detail the causes and the relative contributions of regional patterns precipitation and  
685 geological formations on streamflow partitioning.

686 On the methodological front, there is opportunity to refine the analysis used here to incorporate the statistical  
687 cross-correlation between fast and slow flows in the reconstruction of the FDC for total streamflow, by adopting  
688 generalized approaches (e.g., copulas). In the exploration of the relative contributions of the monsoons, there is  
689 scope to extend the analysis framework to partition the streamflow variability guided by the actual breakdown  
690 into the seasons each year in a more flexible way, as opposed to the static way. This is likely to make the results  
691 of the analysis more robust and less uncertain. Finally, in the process domain, the filter-based separation of total  
692 streamflow into fast and slow flow can be variably impacted by catchment size, introducing some uncertainty into  
693 the partitioning of the FDC of total streamflow into its fast flow and slow flow components. Future work in this  
694 area should explore ways to overcome these methodological shortcomings.

695

## 696 **Appendix**

### 697 **A.1 Baseflow decomposition (Recursive Digital Filter)**

698 The partitioning of total flow ( $Q$ ) into slow flow ( $Q_s$ ) is performed using recursive digital filter technique as  
699 described in Arnold & Allen (1999) and Arnold et al. (1995). Based on the study by Nathan and McMahon (1990),  
700 they found that a coefficient range between 0.9 and 0.95 yielded most acceptable baseflow separation. Therefore,  
701 we have taken the value 0.95 as a coefficient value for this analysis (more discussion is provided at the end of  
702 A.1). This filter is applied to daily streamflow timeseries data for all the gauging stations across the Peninsular  
703 region.

704 The equation of the filter is



705 
$$q_t = \varepsilon q_{t-1} + \frac{(1+\varepsilon)}{2} (Q_t - Q_{t-1})$$
 (A.1)

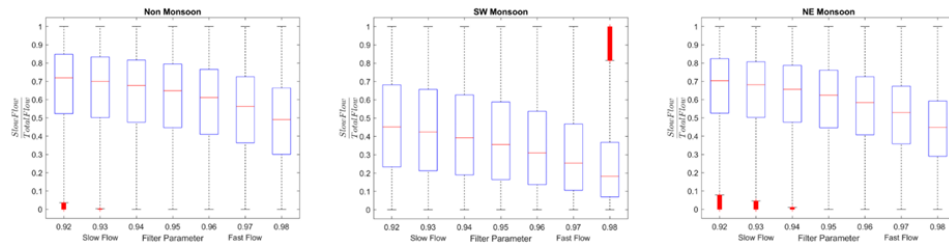
706 where  $q_t$  is the filtered surface runoff (quick response) at the  $t$  time step,  $Q$  is the original streamflow (total flow),  
 707 and  $\varepsilon$  is the filter parameter (which is assumed to be 0.95). Slow flow,  $Q_s$ , is calculated with the equation:

708 
$$Q_s = Q - q_t$$
 (A.2)

709 After obtaining the slow flow component, the fast flow ( $Q_f$ ) is obtained by subtracting  $Q_s$  from  $Q$ .

710 
$$Q_f = Q - Q_s$$
 (A.3)

711 In order to demystify the role of different values of the filter parameter in the digital recursive filter, the model  
 712 was run for three different seasons for all the catchments in Peninsular region. The results are presented in Figure  
 713 A1.



714  
 715 **Figure A1.** Contribution of slow flow to total flow for different seasons. The box plots in each season represent  
 716 the partitioning of total flow into slow flow for different filter parameters, viz. [0.92,0.93,0.94,0.95,0.96,0.97  
 717 ,0.98].  
 718

719 It is observed that the median variations in the slow flow fraction during non-monsoon period (0.5-0.7), south  
 720 west monsoon period (0.18-0.45) and north east monsoon period (0.44-0.7) which lies within 30% variation.  
 721 However, even with these variations, the overall pattern, i.e., high slow flow contribution during non-monsoon  
 722 and north east monsoon seasons and low slow flow contribution during south west monsoon remains intact,  
 723 revealing seasonal changes in the dynamics of slow flow contribution to total flow. In this paper, we assumed the  
 724 parameter 0.95 reflecting the average variability in slow flow contributions to total flow.

#### 725 A.2 Recession Analysis

726 In recession analysis, it is often assumed that rate of change of streamflow  $\frac{dQ}{dt}$  and streamflow ( $Q$ ) follows a  
 727 power law in the form:

728 
$$-\frac{dQ}{dt} = \gamma Q^\beta$$
 (A.4)

729 The parameter  $\gamma$  is function of static watershed properties (i.e., hydrological conductivity, drainable porosity,  
 730 aquifer depth, aquifer breadth, impermeable layer slope and length of stream) (Tashie et al., 2020a). The parameter  
 731  $\beta$  represents the geometry of the contributing aquifer and water table elevation profile that defines the early and  
 732 late periods of recession (Tashie et al., 2020b).  $\frac{dQ}{dt}$  is estimated using exponential time stepping scheme (Roques  
 733 et al., 2017). Strictly decreasing recession segments ( $\frac{dQ}{dt} < 0$ ) with recession segments more than 5 days are  
 734 considered for the estimation of the parameters ( $\gamma$  and  $\beta$ ) (Jachens et al., 2020). A weighted least square  
 735 regression is used to fit a line in log-log space to recession segments (Roques et al., 2017). The median of the  
 736 parameters is used to describe catchment-average recession behaviour (Gnann et al., 2021).



737 **A.3 Absolute contributions of fast and slow flow to total flow**

738 The absolute contributions of fast and slow flow to total flow are determined using the coefficient of determination  
 739 ( $R^2$ ) of simple linear regression models, that measures the reduction in variability of total flow due to fast and  
 740 slow flow components. The details are given below:

741 Model 1:  $Q = \varphi_1 \cdot Q_f + \epsilon_1$  (A.5)

742 Model 2:  $Q = \varphi_2 \cdot Q_s + \epsilon_2$  (A.6)

743 The coefficient of determination measures the effect of slow/fast flow in reducing the variation in total flow  
 744 based on Model1(Model2). Higher the value of this coefficient, higher the contribution of slow/fast flow in  
 745 reducing the variation in total flow.

746 The coefficient of determinations for two models can be estimated as:

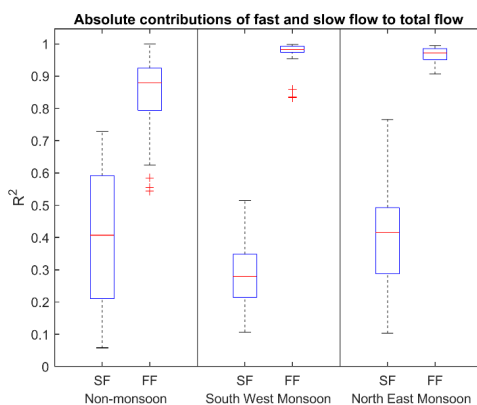
747  $R_{(1)}^2 = \frac{SSR^{(1)}}{SSTO}$  (A.7)

748  $R_{(2)}^2 = \frac{SSR^{(2)}}{SSTO}$  (A.8)

749 where,  $SSR^{(1)}$  and  $SSR^{(2)}$  represent the regression sum of squares for Model 1 and Model 2 respectively, and  
 750 SSTO represents the total sum of squared deviations from mean, i.e.,  $SSTO = \sum(Q_i - \bar{Q})^2$ . The sum of squares  
 751 due to the models are expressed as:

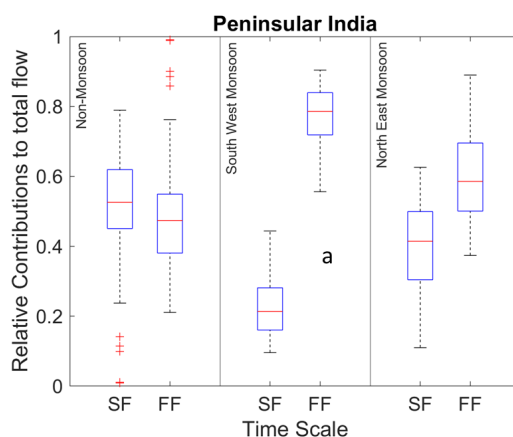
752  $SSR^{(1)} = \sum(\widehat{Q}_{(1)} - \bar{Q})^2$  and  $SSR^{(2)} = \sum(\widehat{Q}_{(2)} - \bar{Q})^2$  where  $\widehat{Q}_{(1)}$  and  $\widehat{Q}_{(2)}$  are the fitted values of total flow using  
 753 Model 1 and Model 2 respectively.

754 The values of coefficient of determination ( $R^2$ ) for three seasons are shown in Fig. A2.



755

756 **Figure A2.** Coefficient of determination representing the absolute contribution of fast/slow flow in reducing the  
 757 variation in total flow across seasons.



758

759 **Figure A3.** Relative contributions of fast (FF) and slow flow (SF) to total flow at regional and seasonal scales  
 760 (NM – Non-monsoon, SW – South-West monsoon and NE – North-East monsoon).

761 It can be shown that the pattern of absolute contribution remains similar (in terms of phase relationship between  
 762 slow and fast flow contributions to total flow) with that of relative contribution as reported in Fig A3. However,  
 763 there are differences in the magnitudes of the absolute contributions and relative contributions of the flow  
 764 components to total flow. The major difference between relative and absolute contribution analyses is that the  
 765 contribution of the fast flow is significantly higher than the slow flow for non-monsoon season, which can be  
 766 attributed to rainfall during the non-monsoon period (Fig 6).

#### 767 A.4 Fitting statistical distributions

768 A simple statistical distribution, the mixed gamma distribution, is employed here to characterize the FDC in  
 769 Peninsular River system. The choice of the mixed gamma distribution is made to take care of the flow regimes of  
 770 the selected basins (i.e., to accommodate the presence of zero flow values) (Cheng et al., 2012). The classic gamma  
 771 distribution is a two-parameter, continuous distribution with a shape parameter,  $k$ , and a scale parameter,  $\theta$ . In  
 772 addition, the probability of zero flows,  $\alpha$ , is defined as the ratio of the number of zero flow days to the total number  
 773 of days within the data record. The mixed gamma distribution (Cheng et al., 2012) employed to model FDC is as  
 774 follows:

$$f(q, k, \theta, \alpha) = \begin{cases} \alpha, & q = 0 \\ (1 - \alpha) \cdot g(q, k, \theta), & q > 0 \end{cases} \quad (\text{A.9})$$

775 where  $g(q, k, \theta)$  is the probability density function of the gamma distribution. The probability density function of  
 776 the gamma distribution is assumed to take the form of (Cheng et al., 2012):

$$g(q, k, \theta) = \frac{1}{|\theta| \Gamma(k)} \left(\frac{q}{\theta}\right)^{k-1} \exp\left(-\frac{q}{\theta}\right) \quad (\text{A.10})$$



777 where  $k$  and  $\theta$  are the shape and scale parameters, respectively. The parameters  $k$  and  $\theta$  can be estimated by the  
 778 method of moments. The mean,  $\mu$ , and variance,  $\nu$ , of the gamma distribution are evaluated from the  $q > 0$  time  
 779 series. The parameters are related to  $\mu$  and  $\nu$  as follows:

$$\mu = k \cdot \theta \quad (\text{A.11})$$

$$\nu = k \cdot \theta^2 \quad (\text{A.12})$$

780 The following formulation is used to obtain the flow given a probability of exceedance,  $p$  (Cheng et al., 2012):

$$q(p, k, \theta, \alpha) = \begin{cases} G^{-1}\left(1 - \frac{p}{1 - \alpha}, k, \theta\right), & 0 \leq p \leq 1 - \alpha \\ 0, & 1 - \alpha < p \leq 1 \end{cases} \quad (\text{A.13})$$

781 where  $G^{-1}$  is the inverse of the CDF of the mixed gamma distribution.

782 In this case, given that we have already looked at the climatic and landscape controls on the mean annual flows,  
 783 we instead work with the normalized daily streamflow time series (i.e., daily streamflow divided by long-term  
 784 mean daily streamflow), which is then used to estimate the parameters of the mixed gamma distribution. The  
 785 parameters estimated from the normalized streamflow series can thus be used to infer secondary controls on the  
 786 shape of flow duration curves.

787

#### 788 A.5 Investigating the slow flow fraction of total flow in Peninsular India

789 The variability in slow flow fraction (SFF) is investigated using multiple linear regression by considering the  
 790 recession parameters,  $\beta$  and  $\gamma$  in the equation  $-\frac{dQ}{dt} = \gamma Q^\beta$  and the location of the gauge ( $\delta$ , latitude). The results  
 791 are provided below:

792 *Regression Model:*

$$SFF = \alpha_0 + \alpha_1\gamma + \alpha_2\beta + \alpha_3\delta \quad (\text{A.14})$$

793

794 **Table A.1** – Statistical Assessment of regression coefficients

Coefficients	Estimate	SE	tStat	pValue
$\alpha_0$ , (Intercept)	0.35361	0.055275	6.3973	2.99E-08
$\alpha_1$	-0.024117	0.021119	-1.142	0.25816
$\alpha_2$	0.12791	0.025704	4.9764	6.12E-06
$\alpha_3$	-0.015556	0.0023978	-6.4875	2.12E-08

795

796 The above regression model was able to explain to about 52% of the variability in slow flow fraction of total flow  
 797 (p-value =  $1.98 \times 10^{-9}$ ), and in general, the model is found to be useful to explain SFF in terms of recession  
 798 parameter and latitude. A fraction of the unexplainable part in SFF can be attributed to the heterogeneity in  
 799 subsurface geologic formations and dam induced variations in the catchment storages. However, at a regional  
 800 scale, the south-north gradient (represented by the parameter  $\delta$ ) can explain the variability in slow flow fraction  
 801 to total flow. This regional setting is an important outcome to understand the streamflow variability in Peninsular  
 802 region of India.

803



804 *Data availability.* The streamflow datasets used for the analysis are accessible from  
805 <https://indiawris.gov.in/wris/#/>. The daily India Meteorological Department (IMD) gridded rainfall product at  
806 spatial resolution of  $0.25^\circ \times 0.25^\circ$   
807 ([https://www.imdpune.gov.in/Clim\\_Pred\\_LRF\\_New/Gridded\\_Data\\_Download.html](https://www.imdpune.gov.in/Clim_Pred_LRF_New/Gridded_Data_Download.html)) from Pai et al., (2014) is  
808 used. The function baseflow, used for partitioning total flow to slow flow is downloaded from  
809 [https://in.mathworks.com/matlabcentral/fileexchange/58525-baseflow-filter-using-the-recursive-digital-filter-](https://in.mathworks.com/matlabcentral/fileexchange/58525-baseflow-filter-using-the-recursive-digital-filter-technique)  
810 [technique](https://in.mathworks.com/matlabcentral/fileexchange/58525-baseflow-filter-using-the-recursive-digital-filter-technique).

811 *Author contributions.* PD, JM, and MS conceptualized the work, developed the methodology, and carried out the  
812 data curation, formal analysis, validation, and writing of the original draft. MS and PPM reviewed the initial  
813 manuscript, and PPM provided the resources needed for this work.

814 *Competing interests.* The authors declare that they have no conflict of interest.

815 *Acknowledgements.* PD acknowledges DST INSPIRE Faculty Fellowship (DST/INSPIRE/04/2022/001952  
816 Faculty Reference No.: IFA22-EAS 114) received from Department of Science and Technology, Government of  
817 India, in Earth and Atmospheric Sciences Division of 2022 call. MS acknowledges the award of a Satish Dhawan  
818 Endowed Visiting Professorship that enabled him to visit the Interdisciplinary Centre for Water Research  
819 (ICWaR) at the Indian Institute of Science, which allowed him to participate in the research activity that  
820 culminated in this paper. MS also acknowledges the generous support and facilities provided by ICWaR that made  
821 his stay a very productive one.

822

## 823 **References**

824 Arnold, J. G. and Allen, P. M.: Automated methods for estimating baseflow and ground water recharge from  
825 streamflow records, *J. Am. Water Resour. Assoc.*, 35, 411–424, [https://doi.org/10.1111/j.1752-](https://doi.org/10.1111/j.1752-1688.1999.tb03599.x)  
826 [1688.1999.tb03599.x](https://doi.org/10.1111/j.1752-1688.1999.tb03599.x), 1999.

827 Arnold, J. G., Allen, P. M., Muttiah, R., and Bernhardt, G.: Automated Base Flow Separation and Recession  
828 Analysis Techniques, *Ground Water*, 33, 1010–1018, <https://doi.org/10.1111/j.1745-6584.1995.tb00046.x>, 1995.

829 Arulbalaji, P., Sreelash, K., Maya, K., and Padmalal, D.: Hydrological assessment of groundwater potential zones  
830 of Cauvery River Basin, India: a geospatial approach, *Environ. Earth Sci.*, 78, 1–21,  
831 <https://doi.org/10.1007/s12665-019-8673-6>, 2019.

832 Basso, S. and Botter, G.: Streamflow variability and optimal capacity of run-of-river hydropower plants, *Water*  
833 *Resour. Res.*, 48, 1–13, <https://doi.org/10.1029/2012WR012017>, 2012.

834 Bhardwaj, K., Shah, D., Aadhar, S., and Mishra, V.: Propagation of Meteorological to Hydrological Droughts in  
835 India, *J. Geophys. Res. Atmos.*, 125, <https://doi.org/10.1029/2020JD033455>, 2020.

836 Biswal, B. and Nagesh Kumar, D.: Study of dynamic behaviour of recession curves, *Hydrol. Process.*, 28, 784–  
837 [792](https://doi.org/10.1002/hyp.9604), <https://doi.org/10.1002/hyp.9604>, 2014.

838 Blum, A. G., Archfield, S. A., Vogel, R. M., and Survey, G.: On the probability distribution of daily streamflow  
839 in the United States, *Hydrol. Earth Syst. Sci.*, 21, 3093–3103, [https://doi.org/https://doi.org/10.5194/hess-21-](https://doi.org/https://doi.org/10.5194/hess-21-3093-2017)  
840 [3093-2017](https://doi.org/https://doi.org/10.5194/hess-21-3093-2017), 2017.

841 Botter, G., Zanardo, S., Porporato, A., Rodriguez-Iturbe, I., and Rinaldo, A.: Ecohydrological model of flow  
842 duration curves and annual minima, *Water Resour. Res.*, 44, 1–12, <https://doi.org/10.1029/2008WR006814>, 2008.

843 Chanapathi, T. and Thatikonda, S.: Investigating the impact of climate and land-use land cover changes on  
844 hydrological predictions over the Krishna river basin under present and future scenarios, *Sci. Total Environ.*, 721,  
845 [137736](https://doi.org/10.1016/j.scitotenv.2020.137736), <https://doi.org/10.1016/j.scitotenv.2020.137736>, 2020.



- 846 Chandra, P. C.: Groundwater of Hard Rock Aquifers of India, 61–84, [https://doi.org/10.1007/978-981-10-3889-1\\_5](https://doi.org/10.1007/978-981-10-3889-1_5), 2018.
- 848 Chatterjee, S., Scotese, C. R., and Bajpai, S.: The Restless Indian plate and its epic voyage from Gondwana to  
849 Asia: Its tectonic, paleoclimatic, and paleobiogeographic evolution, *Spec. Pap. Geol. Soc. Am.*, 529, 1–147,  
850 <https://doi.org/10.1130/2017.2529>, 2017.
- 851 Cheng, L., Yaeger, M., Viglione, A., Coopersmith, E., Ye, S., and Sivapalan, M.: Exploring the physical controls  
852 of regional patterns of flow duration curves &ndash; Part 1: Insights from statistical analyses, *Hydrol. Earth Syst.*  
853 *Sci.*, 16, 4435–4446, <https://doi.org/10.5194/hess-16-4435-2012>, 2012.
- 854 Chouaib, W., Caldwell, P. V., and Alila, Y.: Regional variation of flow duration curves in the eastern United  
855 States: Process-based analyses of the interaction between climate and landscape properties, *J. Hydrol.*, 559, 327–  
856 346, <https://doi.org/10.1016/j.jhydrol.2018.01.037>, 2018.
- 857 Collins, L. S., Loveless, S. E., Muddu, S., Buvaneshwari, S., Palamakumbura, R. N., Krabbendam, M., Lapworth,  
858 D. J., Jackson, C. R., Goody, D. C., Nara, S. N. V., Chattopadhyay, S., and MacDonald, A. M.: Groundwater  
859 connectivity of a sheared gneiss aquifer in the Cauvery River basin, India, *Hydrogeol. J.*, 28, 1371–1388,  
860 <https://doi.org/10.1007/s10040-020-02140-y>, 2020.
- 861 Costa, V. and Fernandes, W.: Regional Modeling of Long-Term and Annual Flow Duration Curves: Reliability  
862 for Information Transfer with Evolutionary Polynomial Regression, *J. Hydrol. Eng.*, 26, 1–12,  
863 [https://doi.org/10.1061/\(asce\)he.1943-5584.0002051](https://doi.org/10.1061/(asce)he.1943-5584.0002051), 2021.
- 864 Das, S.: Frontiers of Hard Rock Hydrogeology in India, in: *Ground Water Development - Issues and Sustainable*  
865 *Solutions*, Springer Singapore, Singapore, 35–68, [https://doi.org/10.1007/978-981-13-1771-2\\_3](https://doi.org/10.1007/978-981-13-1771-2_3), 2019.
- 866 Deshpande, N. R., Kothawale, D. R., and Kulkarni, A.: Changes in climate extremes over major river basins of  
867 India, *Int. J. Climatol.*, 36, 4548–4559, <https://doi.org/10.1002/joc.4651>, 2016.
- 868 Dralle, D., Karst, N., and Thompson, S. E.: a, b careful: The challenge of scale invariance for comparative analyses  
869 in power law models of the streamflow recession, *Geophys. Res. Lett.*, 42, 9285–9293,  
870 <https://doi.org/10.1002/2015GL066007>, 2015.
- 871 Gadgil, S.: The Indian Monsoon and Its Variability, *Annu. Rev. Earth Planet. Sci.*, 31, 429–467,  
872 <https://doi.org/10.1146/annurev.earth.31.100901.141251>, 2003.
- 873 Ghotbi, S., Wang, D., Singh, A., Blöschl, G., and Sivapalan, M.: A New Framework for Exploring Process  
874 Controls of Flow Duration Curves, *Water Resour. Res.*, 56, <https://doi.org/10.1029/2019WR026083>, 2020a.
- 875 Ghotbi, S., Wang, D., Singh, A., Mayo, T., and Sivapalan, M.: Climate and Landscape Controls of Regional  
876 Patterns of Flow Duration Curves Across the Continental United States: Statistical Approach, *Water Resour. Res.*,  
877 56, <https://doi.org/10.1029/2020WR028041>, 2020b.
- 878 Gnann, S. J., McMillan, H. K., Woods, R. A., and Howden, N. J. K.: Including Regional Knowledge Improves  
879 Baseflow Signature Predictions in Large Sample Hydrology, *Water Resour. Res.*, 57,  
880 <https://doi.org/10.1029/2020WR028354>, 2021.
- 881 Gupta, H., Reddy, K. K., Gandla, V., Paridula, L., Chiluka, M., and Vashisth, B.: Freshwater discharge from the  
882 large and coastal peninsular rivers of India: A reassessment for sustainable water management, *Environ. Sci.*  
883 *Pollut. Res.*, 29, 14400–14417, <https://doi.org/10.1007/s11356-021-16811-0>, 2022.
- 884 Harini, P., Sahadevan, D. K., Das, I. C., Manikyamba, C., Durgaprasad, M., and Nandan, M. J.: Regional  
885 Groundwater Assessment of Krishna River Basin Using Integrated GIS Approach, *J. Indian Soc. Remote Sens.*,  
886 46, 1365–1377, <https://doi.org/10.1007/s12524-018-0780-4>, 2018.
- 887 Harman, C. and Troch, P. A.: What makes Darwinian hydrology “Darwinian”? Asking a different kind of question  
888 about landscapes, *Hydrol. Earth Syst. Sci.*, 18, 417–433, <https://doi.org/10.5194/hess-18-417-2014>, 2014.
- 889 Jachens, E. R., Rupp, D. E., Roques, C., and Selker, J. S.: Recession analysis revisited: impacts of climate on  
890 parameter estimation, *Hydrol. Earth Syst. Sci.*, 24, 1159–1170, <https://doi.org/10.5194/hess-24-1159-2020>, 2020.
- 891 Kale, V. S., Hire, P., and Baker, V. R.: Flood Hydrology and Geomorphology of Monsoon-dominated Rivers:  
892 The Indian Peninsula, *Water Int.*, 22, 259–265, <https://doi.org/10.1080/02508069708686717>, 1997.
- 893 Kale, V. S., Vaidyanadhan, R.: *Landscapes and Landforms of India*, edited by: Kale, V. S., Springer Netherlands,



- 894 Dordrecht, 105–113 pp., [https://doi.org/10.1007/978-94-017-8029-2\\_6](https://doi.org/10.1007/978-94-017-8029-2_6), 2014.
- 895 Koneti, S., Sunkara, S. L., and Roy, P. S.: Hydrological modeling with respect to impact of land-use and land-  
896 cover change on the runoff dynamics in Godavari river basin using the HEC-HMS model, *ISPRS Int. J. Geo-*  
897 *Information*, 7, <https://doi.org/10.3390/ijgi7060206>, 2018.
- 898 Krishnamurthy, V. and Ajayamohan, R. S.: Composite Structure of Monsoon Low Pressure Systems and Its  
899 Relation to Indian Rainfall, *J. Clim.*, 23, 4285–4305, <https://doi.org/10.1175/2010JCLI2953.1>, 2010.
- 900 Kumar Raju, B. C. and Nandagiri, L.: Analysis of historical trends in hydrometeorological variables in the upper  
901 Cauvery Basin, Karnataka, India, *Curr. Sci.*, 112, 577–587, <https://doi.org/10.18520/cs/v112/i03/577-587>, 2017.
- 902 Magilligan, F. J. and Nislow, K. H.: Changes in hydrologic regime by dams, *Geomorphology*, 71, 61–78,  
903 <https://doi.org/10.1016/j.geomorph.2004.08.017>, 2005.
- 904 Magilligan, F. J., Nislow, K. H., and Graber, B. E.: Scale-independent assessment of discharge reduction and  
905 riparian disconnectivity following flow regulation by dams, *Geology*, 31, 569, [https://doi.org/10.1130/0091-7613\(2003\)031<0569:SAODRA>2.0.CO;2](https://doi.org/10.1130/0091-7613(2003)031<0569:SAODRA>2.0.CO;2), 2003.
- 907 Milliman JD, F. K.: River discharge to the coastal ocean: a global synthesis, river discharge to the coastal ocean:  
908 a global synthesis, Cambridge University Press, 2011.
- 909 Narasimhan, T. N.: Ground Water in Hard-Rock Areas of Peninsular India: Challenges of Utilization, *Ground*  
910 *Water*, 44, 130–133, <https://doi.org/10.1111/j.1745-6584.2005.00167.x>, 2006.
- 911 Nathan, R. J. and McMahon, T. A.: Evaluation of automated techniques for base flow and recession analyses,  
912 *Water Resour. Res.*, 26, 1465–1473, <https://doi.org/10.1029/WR026i007p01465>, 1990.
- 913 Pai, D. S., Sridhar, L., Rajeevan, M., Sreejith, O. P., Satbhai, N. S., and Mukhopadhyay, B.: Development of a  
914 new high spatial resolution ( $0.25^\circ \times 0.25^\circ$ ) long period (1901–2010) daily gridded rainfall data set over India and  
915 its comparison with existing data sets over the region, *Mausam*, 1, 1–18, 2014.
- 916 Patil, S., Kulkarni, H., Bhave, N., Development, W. R., Forum, P., Dialogue, P., and Conflicts, W.: Groundwater  
917 in the Mahanadi River Basin, <https://doi.org/10.13140/RG.2.2.11561.95846>, 2017.
- 918 Prakash, S., Mitra, A. K., and Pai, D. S.: Comparing two high-resolution gauge-adjusted multisatellite rainfall  
919 products over India for the southwest monsoon period, *Meteorol. Appl.*, 22, 679–688,  
920 <https://doi.org/10.1002/met.1502>, 2015.
- 921 Rajeevan, M., Unnikrishnan, C. K., Bhate, J., Niranjan Kumar, K., and Sreekala, P. P.: Northeast monsoon over  
922 India: variability and prediction, *Meteorol. Appl.*, 19, 226–236, <https://doi.org/10.1002/met.1322>, 2012.
- 923 Ramachandra, T. V.: Global Biodiversity Hotspot - Western Ghats : Water Tower of Peninsular India and Precious  
924 Heritage for Posterity, 2018.
- 925 Rao, P. G., Chanapathi, T., Thatikonda, S., Koneti, S., Sunkara, S. L., Roy, P. S., Kumar Raju, B. C., and  
926 Nandagiri, L.: Investigating the impact of climate and land-use land cover changes on hydrological predictions  
927 over the Krishna river basin under present and future scenarios, *Curr. Sci.*, 7, 577–587,  
928 <https://doi.org/10.18520/cs/v112/i03/577-587>, 2017.
- 929 Rehana, S. and Mujumdar, P. P.: River water quality response under hypothetical climate change scenarios in  
930 Tunga-Bhadra river, India, *Hydrol. Process.*, 25, 3373–3386, <https://doi.org/10.1002/hyp.8057>, 2011.
- 931 Rehana, S. and Mujumdar, P. P.: Climate change induced risk in water quality control problems, *J. Hydrol.*, 444–  
932 445, 63–77, <https://doi.org/10.1016/j.jhydrol.2012.03.042>, 2012.
- 933 Richards, F. D., Hoggard, M. J., and White, N. J.: Cenozoic epeirogeny of the Indian peninsula, *Geochemistry,*  
934 *Geophys. Geosystems*, 17, 4920–4954, <https://doi.org/10.1002/2016GC006545>, 2016.
- 935 Roques, C., Rupp, D. E., and Selker, J. S.: Improved streamflow recession parameter estimation with attention to  
936 calculation of  $-dQ/dt$ , *Adv. Water Resour.*, 108, 29–43, <https://doi.org/10.1016/j.advwatres.2017.07.013>, 2017.
- 937 Saha, K. R., Mooley, D. A., and Saha, S.: The Indian monsoon and its economic impact, *GeoJournal*, 3,  
938 <https://doi.org/10.1007/BF00257706>, 1979.
- 939 Searcy, J. K.: Flowduration curves, *Man. Hydrol. U.S. Geol. Surv.*, 1959.



- 940 Sinha, J., Sharma, A., Khan, M., and Goyal, M. K.: Assessment of the impacts of climatic variability and  
941 anthropogenic stress on hydrologic resilience to warming shifts in Peninsular India, *Sci. Rep.*, 8, 13833,  
942 <https://doi.org/10.1038/s41598-018-32091-0>, 2018.
- 943 Sivapalan, M.: From engineering hydrology to Earth system science: milestones in the transformation of  
944 hydrologic science, *Hydrol. Earth Syst. Sci.*, 22, 1665–1693, <https://doi.org/10.5194/hess-22-1665-2018>, 2018.
- 945 Smakhtin, V. U.: Smakhtin 2010- Low flow hydrology.pdf, *J. Hydrol. Hydrol.*, 240, 147–186,  
946 [https://doi.org/10.1016/S0022-1694\(00\)00340-1](https://doi.org/10.1016/S0022-1694(00)00340-1), 2001.
- 947 Sreelash, K., Mathew, M. M., Nisha, N., Arulbalaji, P., Bindu, A. G., and Sharma, R. K.: Changes in the  
948 hydrological characteristics of Cauvery river draining the eastern side of southern Western Ghats, India, *Int. J.*  
949 *River Basin Manag.*, 18, 153–166, <https://doi.org/10.1080/15715124.2020.1719119>, 2020.
- 950 Tashie, A., Pavelsky, T., and Band, L. E.: An Empirical Reevaluation of Streamflow Recession Analysis at the  
951 Continental Scale, *Water Resour. Res.*, 56, <https://doi.org/10.1029/2019WR025448>, 2020a.
- 952 Tashie, A., Pavelsky, T., and Emanuel, R. E.: Spatial and Temporal Patterns in Baseflow Recession in the  
953 Continental United States, *Water Resour. Res.*, 56, <https://doi.org/10.1029/2019WR026425>, 2020b.
- 954 Tongal, H., Demirel, M. C., and Moradkhani, H.: Analysis of dam-induced cyclic patterns on river flow dynamics,  
955 *Hydrol. Sci. J.*, 62, 626–641, <https://doi.org/10.1080/02626667.2016.1252841>, 2017.
- 956 Vogel, R. M. and Fennessey, N. M.: Flow-Duration Curves. I: New Interpretation and Confidence Intervals, *J.*  
957 *Water Resour. Plan. Manag.*, 120, 485–504, [https://doi.org/10.1061/\(ASCE\)0733-9496\(1994\)120:4\(485\)](https://doi.org/10.1061/(ASCE)0733-9496(1994)120:4(485)), 1994.
- 958 Vogel, R. M. and Fennessey, N. M.: Flow Duration Curves II: a Review of Applications in Water Resources  
959 Planning, *JAWRA J. Am. Water Resour. Assoc.*, 31, 1029–1039, <https://doi.org/10.1111/j.1752-1688.1995.tb03419.x>, 1995.
- 961 Wagener, T., Blöschl, G., Goodrich, D. C., Gupta, H. V., Sivapalan, M., Tachikawa, Y., Troch, P. A., and Weiler,  
962 M.: A synthesis framework for runoff prediction in ungauged basins, in: *Runoff Prediction in Ungauged Basins*,  
963 Cambridge University Press, 11–28, <https://doi.org/10.1017/CBO9781139235761.005>, 2013.
- 964 Yokoo, Y. and Sivapalan, M.: Towards reconstruction of the flow duration curve: Development of a conceptual  
965 framework with a physical basis, *Hydrol. Earth Syst. Sci.*, 15, 2805–2819, [https://doi.org/10.5194/hess-15-2805-](https://doi.org/10.5194/hess-15-2805-2011)  
966 2011, 2011.
- 967